Chapter 13
Phased Array Radar Antennas

Joe Frank

Johns Hopkins University Applied Physics Laboratory

John D. Richards

Johns Hopkins University Applied Physics Laboratory

13.1 INTRODUCTION*

Phased Array Radars. Early radar systems used antenna arrays formed by the combination of individual radiators. Such antennas date back to the turn of the twentieth century.[1,2,3] Antenna characteristics are determined by the geometric position of the radiators and the amplitude and phase of their excitation. As radars progressed to shorter wavelengths, arrays were displaced by simpler antennas such as parabolic reflectors. For modern radar applications, the advent of electronically controlled phase shifters, switches, and transmit/receive modules has once more directed attention to array antennas. The aperture excitation may now be modulated by controlling the phase of the individual elements to give beams that are scanned electronically. The dramatic advantage of electronically steered phased arrays as compared to reflectors is provided by the time required to steer beams and the flexibility in steering. While prior radars took seconds to steer to a new location, phased arrays take microseconds. In addition, the new location can be anywhere in a hemisphere. This chapter will be devoted to arrays of this type.

Multifunction Radar. The capability of rapidly and accurately switching beams permits multiple radar functions to be performed, interlaced in time. An electronically steered array radar may track a great multiplicity of targets, illuminate a number of targets with RF energy and guide missiles toward them, and perform complete hemispherical search with automatic target selection and handover to tracking. It may even act as a communication system, directing high-gain beams toward distant receivers and transmitters. Complete flexibility is possible; search and track rates may be adjusted to best meet particular situations, all within the limitations set by the total use of time.

* Portions of this chapter that appeared in earlier editions of the *Radar Handbook* were written by the late Theodore C. Cheston, a pioneer in phased array antennas.

The antenna beamwidth may be changed to search some areas more rapidly with less gain. Frequency agility is possible with the frequency of transmission changing at will from pulse to pulse or, with coding, within a pulse. Very high powers may be generated from a multiplicity of amplifiers distributed across the aperture. Electronically controlled array antennas can give radars the flexibility needed to perform all the various functions in a way best suited for the specific task at hand. The functions may be programmed adaptively to the limit of one's capability to exercise effective automatic management and control.

Phased array theory was studied intensively in the 1960s. Technology advanced and led to a series of operational systems in the 1980s; many publications became available.[4–15] In terms of performance improvement, ultralow sidelobes (less than –40 dB) were demonstrated first in the 1970s by Westinghouse Electric Corporation's AWACS (Airborne Warning and Control System) and brought about tight tolerances in construction and phase settings. The advent of more and better computer modeling and sophisticated test equipment such as network analyzers has led to improved methods of designing well-matched apertures. Better components such as radiating elements, phase shifters, and power dividers are now available. More economical solid-state devices and memory chips have led to precision aperture phase control with corrections for frequency and temperature variations. Solid-state microwave devices hold great promise for future systems where a solid-state module is associated with each radiating element; improvements in terms of aperture control, reliability, and efficiency continue. Phased arrays can be controlled adaptively, particularly for sidelobe cancellation. This is an area where theory and understanding have advanced much. Also great progress has been made with indoor near-field antenna ranges,[16] where computer-controlled precision two-dimensional radiation patterns are derived at multiple frequencies and with scanning.

Phased arrays are very expensive. As technology advances, costs are expected to be reduced. At the same time, the quest for better performance with lower sidelobes and wider bandwidth keeps the costs high.

Phased Array Antennas. The phased array antenna has an aperture that is assembled from a great many similar radiating elements, such as slots, dipoles, or patches, each element being individually controlled in phase and amplitude. Accurately predictable radiation patterns and beam-pointing directions can be achieved.

The general planar array characteristics are readily obtained from a few simple equations that are given here but discussed later in greater detail. With the elements spaced by $\lambda/2$ (λ = wavelength) to avoid the generation of multiple beams (grating lobes), the number of radiating elements N for a pencil beam is approximately related to the beamwidth by

$$N \approx \frac{10{,}000}{(\theta_B)^2}$$

$$\theta_B \approx \frac{100}{\sqrt{N}}$$

where θ_B is the 3-dB beamwidth in degrees. The corresponding antenna gain, when the beam points broadside to the aperture, is

$$G_0 \approx \pi N \eta \approx \pi N \eta_L \eta_a$$

where η accounts for antenna losses (η_L) and reduction in gain due to unequal weighting of the elements with a nonuniform amplitude (η_a). When scanning to an angle is θ_0, the gain of a planar array is reduced to that of the projected aperture:

$$G(\theta_0) \approx \pi N \eta \cos \theta_0$$

Similarly, the scanned beamwidth is increased from the broadside beamwidth (except in the vicinity of endfire, $\theta_0 = 90°$):

$$\theta_B(\text{scanned}) \approx \frac{\theta_B(\text{broadside})}{\cos \theta_0}$$

The total number of beams M (with broadside beamwidth and square stacking) that fit into a sphere is approximately equal to the gain and with $\eta \approx 1$ is thus simply related to N by

$$M \approx \pi N$$

An array where the elements are fed in parallel (see Section 13.8) and scanned by phase shift, modulo 2π, has limited bandwidth; for wideband operation, constant path lengths rather than constant phases are required. The limit is given by

$$\text{Bandwidth (\%)} \approx \text{beamwidth (°)}$$

This is equivalent to limitations given by

$$\text{Pulse length} = 2 \times \text{aperture size}$$

With these criteria, the scanned radiation pattern at 60° is steered by ± one-fourth of the beamwidth at the angle of scan as the frequency is changed over the band. If all the frequencies in the band are used with equal weighting, then twice the bandwidth (half the pulse length) becomes acceptable. At a scan angle θ_0, the beam steers with frequency through an angle $\delta\theta$ so that

$$\delta\theta \approx \frac{\delta f}{f} \tan \theta_0 \qquad \text{(rad)}$$

For wider bandwidths, time-delay networks have to be introduced to supplement the phase shifters.

Conformal Arrays.[17,18] Phased arrays may conform to curved surfaces as required, for example, for flush-mounting on aircraft or missiles. If the surface has a large radius of curvature so that all the radiating elements point in substantially the same direction, then the characteristics are similar to those of a planar array even though the exact 3D position of the element has to be taken into account to calculate the required phase. A small radius of curvature is found with cylindrical (or spherical) arrays used for 360° coverage. Elements are switched to avoid sections of the antenna where they point away from the desired beam direction. Difficulties may be encountered in matching the radiating elements and in maintaining polarization purity. The discussion in this chapter will concentrate on planar phased arrays, rather than conformal arrays.

3D Volumetric Search. Three-dimensional (3D) volumetric radar search is possible with electronic scanning in both azimuth and elevation; important regions (e.g., the horizon) may be emphasized at will and searched more frequently. The radar may operate with a higher than normal false-alarm rate since targets can easily be confirmed by additional dwells. Phase control allows beams to be widened, for example, to reduce search time for the more elevated regions, where reduced ranges need less antenna gain. A separate rotating surveillance radar system may be added for extra coverage (at a second frequency) and to allow the 3D radar more time for tracking.

Monopulse Track. Phased array radars are well suited for monopulse tracking. The radiating elements of the array can be combined in three different ways to give the sum pattern and the azimuth and elevation difference patterns. Contradictory requirements in optimum amplitude distribution for sum and difference patterns exist,[19] but, as with other antenna systems, they may be independently satisfied. The sum and difference patterns are scanned simultaneously.

The difference-pattern null in a phased array system gives good beam-pointing accuracy. Absolute beam-pointing accuracies to within less than one-fiftieth of a (scanned) beamwidth have been measured with scans up to 60°.[20] The accuracy is limited by phase and amplitude errors. Since phase shift rather than time delay is used, as the frequency is changed, the direction of the null of the scanned beam is also changed, and the beam moves toward broadside with an increase in frequency.

Shaped Beams. The radiation pattern of an array may be shaped by modifying the aperture distribution. Good pattern approximations can be obtained by using phase only. In particular, the beam may be broadened by applying a spherical phase distribution to the aperture or by approximating it with a gable (triangular) phase distribution. Beams of this type are of particular interest because they are easily generated. They may be used for transmission in a system where the receiving antenna has a cluster of simultaneous beams, or, as previously discussed, they may be used in a search system to reduce the number of angular cells in regions of shorter range.

Monitoring. Electronically scanned arrays are composed of very many parts and include electronic circuitry to drive the phase shifters or switches that steer the beam. The overall reliability of such arrays can be great; graceful degradation has been claimed because the failure of as much as 10% of the components leads to a loss in gain of only 1 dB. There is, however, a degradation of (low) sidelobes. Nevertheless, the functioning of the antenna is complex, and there is need for providing test or monitoring circuitry. The decision to point a beam in a certain direction is made somewhere in the radar control system and is normally defined by two direction cosines. A test or monitoring circuit should establish the correct functioning of all components, including all beam-pointing computations, electronic drivers and phase shifters or switches, and all their interconnections. Frequent indications that the antenna system is functioning or is capable of functioning should be available. In one possible method, the phase shifters are programmed to focus on a nearby monitor probe and scan past it.[21] This will yield a close approximation of the complete radiation pattern, where gain and sidelobes can be measured and compared with previous results. The combination of individual elements and their phase shifters (and drivers) can also be checked with this configuration. The phase at each element is sequentially rotated at some low frequency; the amplitude and phase of this modulation as received by the probe relate directly to both the relative amplitude excitation of the element and its

relative phase setting.[22] Other methods have been proposed[23] where measurements are compared with previously recorded ones.

Deployment of Apertures. With planar arrays, scanning is limited by the loss in gain and the increase in beamwidth corresponding to the reduction of the aperture to its projected area. Practical extreme values of scanning are therefore in the region of 60 to 70°. A minimum of three planar array apertures is then necessary for hemispherical coverage. The antennas may be positioned as shown in Figure 13.1, permitting a view that is unimpeded by the central superstructure. The apertures would normally be tilted back from the vertical to balance the scan angles.

Radiating Elements. The most commonly used radiators for phased arrays are dipoles, slots, open-ended waveguides (or small horns), and printed-circuit "patches" (originally called *Collings radiator* after their inventor[24]). The element has to be small enough to fit in the array geometry, thereby limiting the element to an area of a little more than $\lambda^2/4$. In addition, many radiators are required, and the radiating element should be inexpensive and reliable and have identical characteristics from unit to unit.

Because the impedance and pattern of a radiator in an array are determined predominantly by the array geometry (Section 13.4), the radiating element may be chosen to suit the feed system and the physical requirements of the antenna. For example, if the radiator is fed from a stripline phase shifter, a stripline dipole would be a logical choice. If a waveguide phase shifter is used, an open-ended waveguide or a slot might be convenient. At the lower frequencies, where coaxial components are prevalent, dipoles have been favored. A ground plane is usually placed about $\lambda/4$ behind an array of parallel dipoles so that the antenna forms a beam in only one hemisphere.

For limited scanning (say, less than 10°), it is possible to use directive radiators having dimensions of height and width of several wavelengths. With such separation, the mutual coupling effects (see Section 13.4) can be small, and the pattern and impedance of an element in the array approach those of the isolated element.

FIGURE 13.1 Guided missile cruiser showing two out of four phased array antennas (*Courtesy of Ingalls Shipbuilding Division of Litton*)

The element must be chosen to give the desired polarization, usually vertical or horizontal. The special case of circular polarization is discussed below.

If polarization diversity is required or if an array is required to transmit one polarization and receive the orthogonal or both polarizations, either crossed dipoles or circular or square radiators seem suitable. With appropriate feed systems, both are capable of providing vertical and horizontal polarization independently and may be combined to provide any desired polarization, including circular. Such polarization diversity adds considerable complexity, requiring two feed systems or switches at the radiating element level.

Circular Polarization. From the point of view of the antenna designer, circular polarization is possible, though difficulties may be encountered in matching for large scan angles. On scanning, a component of the undesired orthogonal polarization will be generated,[25] and some provision should be made to absorb that energy.[26] With a conventional circularly polarized antenna, such as a parabolic dish with a circularly polarized feed, good circularity may be obtained over part of the main beam, with rapid deterioration over the rest of the pattern. With a planar array, the relevant beamwidth is the beamwidth of the element in the array rather than the array beamwidth.

With circular polarization, the signal returned from a single-bounce target (i.e., a sphere or flat plate) will require an antenna matched to the opposite sense of circular polarization from that transmitted. If the same antenna is used, then single-bounce targets are rejected. Such a system can, therefore, give a measure of suppression of rain echoes,[27] ideally amounting to

$$20 \log (e^2 + 1)/(e^2 - 1) \quad \text{dB}$$

where e is the voltage-ellipticity ratio. An early model of a Raytheon reflectarray gave an ellipticity ratio of less than 1.5 dB with scans up to 30°, corresponding to a theoretical rain rejection of at least 15 dB. At the same time, an aircraft target would typically lose approximately 3 dB, leaving a relative net improvement of 12 dB of rain rejection.

Phased Arrays with Very Wide Bandwidth. A radar system that has the capability of changing frequency over a very wide bandwidth can, with advantage, adapt its transmission to take into account frequency-dependent multipath characteristics, target response, environmental conditions, interference, and jamming. Further, wideband processing can give fine range resolution.

Phased arrays have the potential of operating over very wide bandwidths. The high end of the frequency band is limited by the physical size of the elements, which must be spaced close enough in the array to avoid the generation of grating lobes (see Section 13.2). For wide instantaneous bandwidth (rather than tunable bandwidth), time delays have to be added to prevent the beam from being scanned as the frequency is changed.

The impedance of the radiating element at the aperture (with closely spaced elements) is approximately independent of frequency, but the element must be matched over the wide bandwidth. This is difficult to achieve without exciting harmful surface waves when scanning. Nevertheless, matching with octave bandwidth for scanning to ±60° has been achieved.

Limited Scanning.[28] If scanning is limited to a small angular volume, considerable simplifications become possible. The total number of active controls can be reduced to

about equal the total number of beams. Subarrays (see Section 13.8) may be formed, each with only one phase control of a size such that the subarray beamwidth includes all the scan angles. Alternatively, a small phased array could be placed in the focal region of a large reflector to scan the narrow beamwidth of the reflector over a limited scan angle.

Scanning of Arrays

Phase Scanning. The beam of an antenna points in a direction that is normal to the radiated phase front. In phased arrays, this phase front is adjusted to steer the beam by individual control of the phase of excitation of each radiating element. This is indicated in Figure 13.2*a*. The phase shifters are electronically actuated to permit rapid scanning and are adjusted in phase to a value between 0 and 2π rad. With an interelement spacing s, the incremental phase shift ψ between adjacent elements for a scan angle θ_0 is $\psi = (2\pi/\lambda)s \sin \theta_0$. If the phase ψ is constant with frequency, the scan angle θ_0 is frequency-dependent.

Time-Delay Scanning. Phase scanning was seen to be frequency-sensitive; however, time-delay scanning is independent of frequency. Delay lines are used instead of phase shifters, as shown in Figure 13.2*b*, providing an incremental delay from element to element of $\tau = (s/c) \sin \theta_0$, where c = velocity of propagation. Individual time-delay circuits (Section 13.7) are normally too cumbersome to be added to each radiating element. A reasonable compromise may be reached by adding one time-delay network to a group of elements (subarray) where each element has its own phase shifter.

Frequency Scanning.[29] Frequency rather than phase may be used as the active parameter to exploit the frequency-sensitive characteristics of phase scanning. Figure 13.2*c* shows the arrangement. At one particular frequency, all radiators are in phase. As the frequency is changed, the phase across the aperture tilts linearly, and the beam is scanned. Frequency-scanning arrays are relatively simple and inexpensive

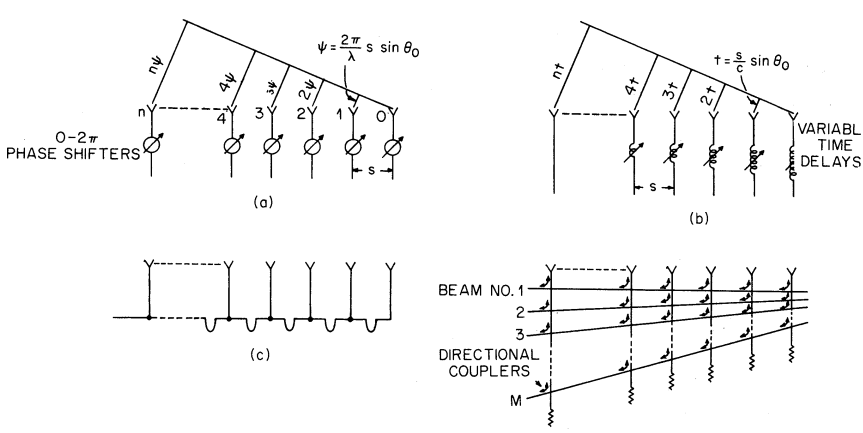

FIGURE 13.2 Generation of scanned beams: (*a*) phased array, (*b*) time-delay array, (*c*) frequency-scanned array, and (*d*) Blass-type array

to implement. They have been developed and deployed in the past to provide elevation-angle scanning in combination with mechanical horizontal rotation for 3D radars. A chapter in the first edition of this handbook was devoted to this approach, which since then has received much less attention; frequency is too important a parameter for achieving high-range resolution, electronic counter-countermeasures, and multiple radar occupancy to give it up for antenna scanning. Frequency scanning is seldom used anymore.

IF Scanning. For receiving, the output from each radiating element may be heterodyned (mixed) to an intermediate frequency (IF). All the various methods of scanning are then possible, including the beam-switching system described below, and can be carried out at IF, where amplification is readily available and lumped constant circuits may be used.

Digital Beamforming.[30–32] For receiving, the output from each radiating element may be amplified and digitized. The signal is then transferred to a computer for processing, which can include the formation of multiple simultaneous beams (formed with appropriate aperture illumination weighting) and adaptively derived nulls in the beam patterns to avoid spatial interference or jamming. Limitations are due to the availability and cost of analog-to-digital (A/D) converters and to their frequency and dynamic-range characteristics. Partial implementation is possible by digitizing at subarray levels only.

Beam Switching. With properly designed lenses or reflectors, a number of independent beams may be formed by feeds at the focal surface. Each beam has substantially the gain and beamwidth of the whole antenna. Allen[33] has shown that there are efficient equivalent transmission networks that use directional couplers and have the same collimating property. A typical form, after Blass,[34] is shown in Figure 13.2*d*. The geometry can be adjusted to provide equal path lengths, thus providing frequency-independent time-delay scanning. Another possible configuration providing multiple broadband beams uses parallel plates containing a wide-angle microwave lens.[35,36] Each port corresponds to a separate beam. The lens provides appropriate time delays to the aperture, giving frequency-invariant scanning. The beams may be selected through a switching matrix requiring $M - 1$ single-pole–double-throw (SPDT) switches to select one out of M beams. The beams are stationary in space and overlap at approximately the 4 dB points. This is in contrast to the previously discussed methods of scanning, where the beam can be steered accurately to any position. The beams all lie in one plane. The system may be combined with mechanical rotation of the antenna, giving vertical-switched scanning for 3D coverage. Much greater complexity is required for a system switching beams in both planes.

Multiple Simultaneous Beams. Instead of switching the beams, as described in the preceding paragraph, all the beams may be connected to separate receivers, giving multiple simultaneous receive beams. The transmitter radiation pattern would need to be wide to cover all the receive beams. Such multibeam systems have found application in combination with mechanical rotation for 3D coverage.

Multiple Independently Steered Beams. Independent multiple beams may be generated with a single beamformer by modifying both amplitude and phase at the aperture. This can be seen from Figure 13.3, where, for example, two independent

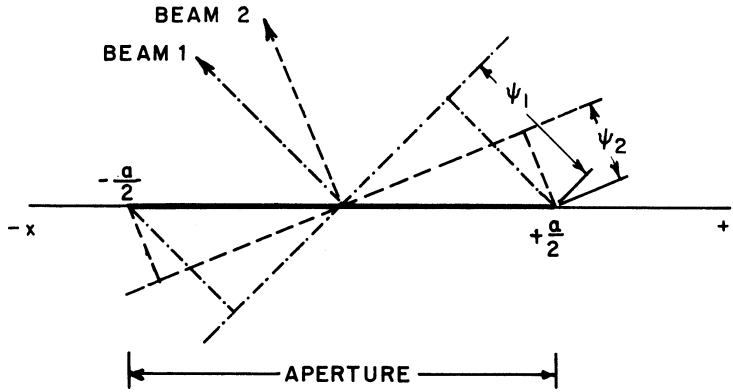

FIGURE 13.3 Aperture distribution giving two beams

beams are generated. Both beams have the same amplitude (voltage) distribution $F(x)$ but differently inclined linear phased fronts. The total aperture excitation with both beams is

$$F(x,\psi) = F(x)e^{j2\psi_1(x/a)} + F(x)e^{j2\psi_2(x/a)} = 2F(x)\cos\left[(\psi_1 - \psi_2)\frac{x}{a}\right]e^{j(\psi_1+\psi_2)(x/a)}$$

That is, the aperture amplitude distribution required for two separate beams varies cosinusoidally, and the phase distribution is linear and has the average inclination.

In most phased array systems, only the phase can be controlled. Ignoring the required amplitude variations still leads to good approximations for forming multiple beams, by superimposing the various required phase-shifter settings (modulo 2π). In the case of two beams, the aperture phase slope has the average inclination and varies periodically from 0 to π.

Vertical Scan Only. A greatly simplified phased array system becomes possible if there is no need for multifunction capabilities, including fire control, where a beam may have to be pointed in any given direction at any time. The array is scanned in the vertical plane only and mechanically rotated to give azimuth coverage. The number of phase control points is then reduced to the number of horizontal rows. In the case of a ship's surveillance radar, the antenna should be positioned as high as possible to avoid shadowing by the superstructure, but the pedestal need not be stabilized since stabilization can be achieved by electronic beam steering. Scanning can be in the form of phase scanning or multiple simultaneous beams may be used on receive with a wide antenna pattern on transmit.

13.2 ARRAY THEORY

Array with Two Elements. Figure 13.4 shows two isotropic radiators that are spaced by a distance s and excited with equal amplitude and phase. With unity input

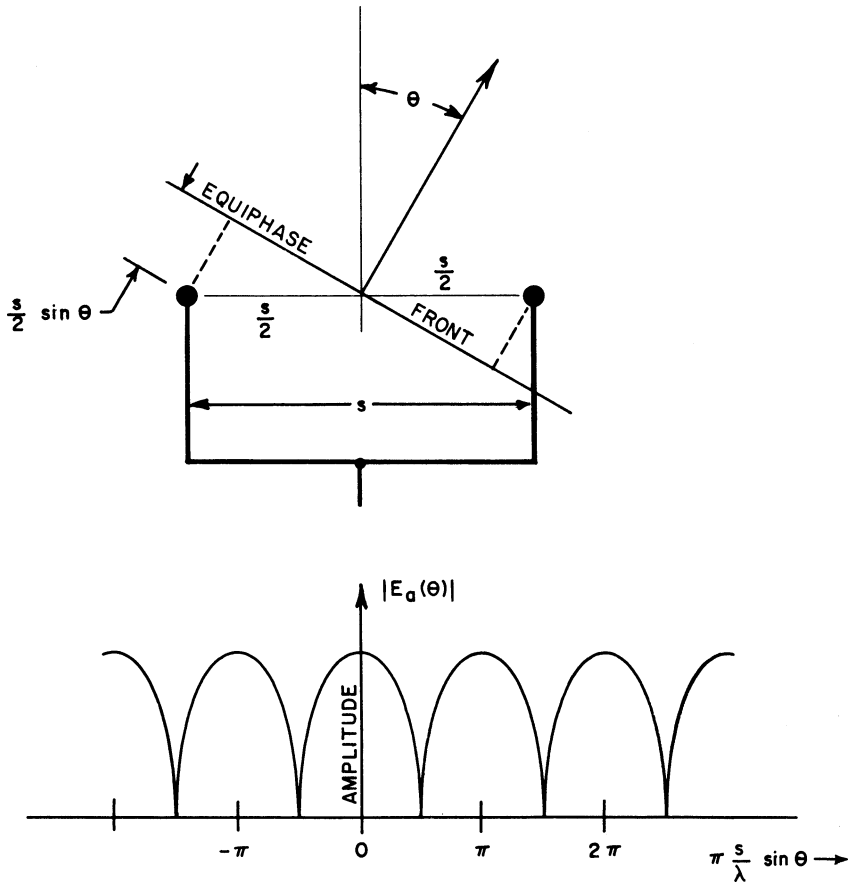

FIGURE 13.4 Radiation pattern of two isotropic radiators

power, the vector sum of their contributions, added at a great distance as a function of θ, is the radiation pattern

$$E_a(\theta) = \frac{1}{\sqrt{2}}[e^{j(2\pi/\lambda)(s/2)\sin\theta} + e^{-j(2\pi/\lambda((s/2)\sin\theta}]$$

where θ is measured from the broadside direction. Normalizing, to get unity amplitude when $\theta = 0$, and simplifying give

$$E_a(\theta) = \cos\left[\pi \frac{s}{\lambda} \sin\theta\right] \tag{13.1}$$

The absolute value of $E_a(\theta)$ is plotted in Figure 13.4 as a function of $\pi(s/\lambda)\sin\theta$. If the plot had been in terms of the angle θ, the lobes would have been found to increase in width as $|\theta|$ increased. The main beam occurs when $\sin\theta = 0$. The other lobes have the same amplitude as the main beam and are referred to as *grating lobes*.

They occur at angles given by $\sin\theta = \pm [m/(s/\lambda)]$, where m is an integer. For the half space given by $-90° < \theta < +90°$, there are $2m'$ grating lobes, where m' is the largest integer smaller than s/λ. If $s < \lambda$, grating-lobe maxima do not occur, and the value at $\pm 90°$ is $\cos(\pi s/\lambda)$. This value is for isotropic radiators and is reduced if the radiators have directivity.

Linear Array.[37] With a linear array of N isotropic radiators, excited with equal amplitudes and phase and separated by distances s, as shown in Figure 13.5, the condition for the occurrence of grating lobes is unchanged from the simpler case just considered. They occur for the same values of $\pi(s/\lambda)\sin\theta$, but the width of the lobes is reduced, and they are separated by minor lobes. Summing the vector contributions from all elements, with element 0 as phase reference, gives

$$E_a(\theta) = \frac{1}{\sqrt{N}} \sum_{n=0}^{n=N-1} e^{j(2\pi/\lambda)\, ns \quad \sin\theta}$$

The factor $1/\sqrt{N}$ shows that each element is energized with $1/N$ of the (unity) input power. Normalizing the gain to unity at broadside, $\theta = 0$, gives the pattern

$$E_a(\theta) = \frac{\sin[N\pi(s/\lambda)\sin\theta]}{N\sin[\pi(s/\lambda)\sin\theta]} \tag{13.2}$$

$E_a(\theta)$ gives the radiation pattern for isotropic radiators and is known as the *array factor*. It is shown in Figure 13.6 for $N = 10$. This pattern is repetitive, and the locations of the adjacent grating lobes at angles θ_1 and θ_2 are separated by $\pi(s/\lambda)(\sin\theta_1 - \sin\theta_2) = \pi$.

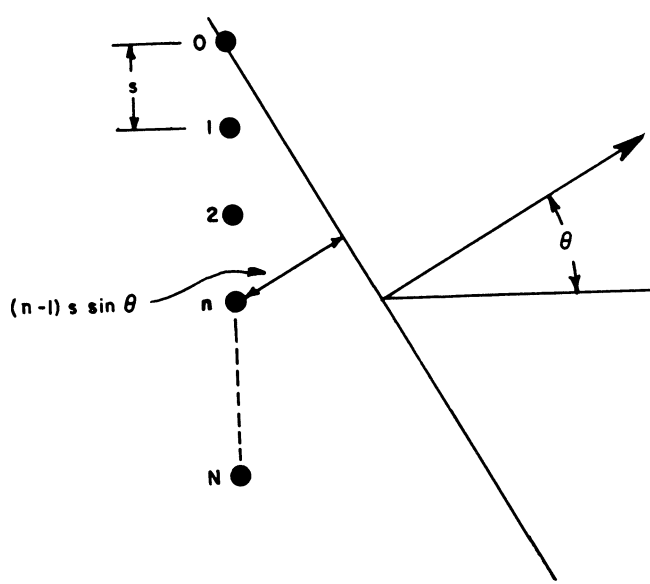

FIGURE 13.5 Linear array with N radiators uniformly spaced by a distance s

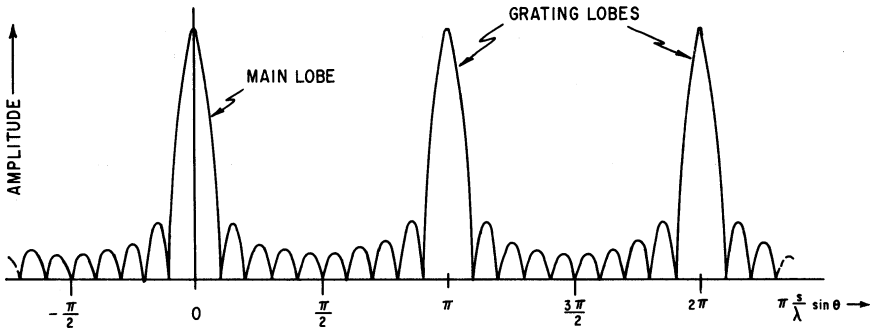

FIGURE 13.6 Array factor with $N = 10$ elements

The radiating elements are not isotropic but have a radiation pattern $E_e(\theta)$, known as the *element factor* or *element pattern*; then the complete radiation pattern $E(\theta)$ is the product of the array factor and the element pattern:

$$E(\theta) = E_e(\theta)E_a(\theta) = E_e(\theta)\frac{\sin[N\pi(s/\lambda)\sin\theta]}{N\sin[\pi(s/\lambda)\sin\theta]} \tag{13.3}$$

An approximation to the pattern of Eq. 13.2 is in the form

$$E(\theta) = \frac{\sin[\pi(a/\lambda)\sin\theta]}{\pi(a/\lambda)\sin\theta} \tag{13.4}$$

where the effective aperture is $a = Ns$, which extends by $s/2$ beyond the centers of the end elements. In contrast to the array factor, this pattern has only one maximum and is nonrepetitive. It is the well-known Fourier transform of a continuous constant-amplitude distribution. For uniform illumination, the beamwidth is

$$\theta_B = \frac{0.886}{a/\lambda}(\text{rad}) = \frac{50.8}{a/\lambda}(^\circ) \tag{13.5}$$

The first sidelobe is 13.3 dB down from the peak of the main beam.

For larger values of θ, the pattern of a continuous aperture is modified from Eq. 13.4 by the obliquity factor[38,39] $1/2\ (1 + \cos\theta)$. This gives

$$E(\theta) = \tfrac{1}{2}(1+\cos\theta)\frac{\sin[\pi(a/\lambda)\sin\theta]}{\pi(a/\lambda)\sin\theta} \tag{13.6}$$

For closely spaced elements, the obliquity factor is very similar to the amplitude pattern of a well-designed (matched) radiating element, $\sqrt{\cos\theta}$, for values up to some 60 or 70°. At greater angles, the element pattern has values that are greater than those given by $\sqrt{\cos\theta}$ and that are a function of the total number of elements.[40]

Scanned Linear Arrays. The pattern of the array may be steered to an angle θ_0 by applying linearly progressive phase increments from element to element so that the phase between adjacent elements differs by $2\pi(s/\lambda)\sin\theta_0$. Equation 13.2 is then modified, giving the normalized array factor of a uniformly illuminated arrays as

$$E_a(\theta) = \frac{\sin N\pi(s/\lambda)(\sin\theta - \sin\theta_0)}{N \sin \pi(s/\lambda)(\sin\theta - \sin\theta_0)} \tag{13.7}$$

and the pattern is

$$E(\theta) = E_e(\theta)\frac{\sin N\pi(s/\lambda)(\sin\theta - \sin\theta_0)}{N \sin[\pi(s/\lambda)(\sin\theta - \sin\theta_0)]} \tag{13.8}$$

Equation 13.8 describes the fundamental response of a scanned array system. The array will have only one single major lobe, and grating-lobe maxima will not occur for $-90° < \theta < +90°$ as long as

$$\pi\frac{s}{\lambda}|\sin\theta - \sin\theta_0| < \pi$$

or

$$\frac{s}{\lambda} < \frac{1}{1+|\sin\theta_0|} \tag{13.9}$$

which is always true if $s/\lambda < ½$. When scanning is limited, the value of s/λ may be increased, for example, to $s/\lambda < 0.53$ for scanning to a maximum of 60° or $s/\lambda < 0.59$ for scanning to a maximum of ±45°.

For larger values of s/λ, grating lobes occur at angles θ_1, given by

$$\sin\theta_1 = \sin\theta_0 \pm \frac{n}{s/\lambda} \tag{13.10}$$

when n is an integer.

In the limit, the inequality (Eq. 13.9) does allow a grating-lobe peak to occur at 90° when scanning to θ_0. Even though the grating lobe is reduced when multiplied by the element pattern, it may be prudent to space the elements such that the first null of the grating lobe, rather than the peak, occurs at 90°. With N elements this more restrictive condition is given by

$$\frac{s}{\lambda} < \frac{N-1}{N} \times \frac{1}{1+|\sin\theta_0|} \tag{13.11}$$

Equation 13.8 may again be approximated by the Fourier transform of the illumination across the continuous aperture:

$$E(\theta) = ½(1+\cos\theta)\frac{\sin \pi(a/\lambda)(\sin\theta - \sin\theta_0)}{\pi(a/\lambda)(\sin\theta - \sin\theta_0)} \tag{13.12}$$

The Fourier-transform solutions for continuous apertures[19,41] may be used to approximate patterns for practical amplitude and phase distributions as long as the element-to-element spacing is small enough to suppress grating lobes.[42] Monopulse difference patterns may be approximated in the same way from the Fourier transforms of the corresponding continuous odd aperture distributions.

Element Factor and Gain of Planar Arrays. The maximum gain of a uniformly illuminated and lossless aperture of area A, with a broadside beam, is $G_{\max} = 4\pi A/\lambda^2$.

With a nonuniform aperture distribution and with losses present, the gain is reduced by the efficiency term η to

$$G_{\max} = 4\pi \frac{A}{\lambda^2} \eta \tag{13.13}$$

If the aperture is considered as a matched receiver, then the amount of energy arriving from a direction θ_0 is proportional to its projected area. The gain with scanning, therefore, is

$$G(\theta_0) = 4\pi \frac{A \cos \theta_0}{\lambda^2} \eta \tag{13.14}$$

If the aperture is made up of N equal radiating elements and is matched to accept the incident power, then the contribution to the overall gain is the same from all elements, hence

$$G(\theta) = NG_e(\theta)\eta \tag{13.15}$$

where G_e is the gain per element. It follows from Eq. 13.14 that the matched element power pattern is

$$G_e(\theta) = 4\pi \frac{A}{N\lambda^2} \cos \theta \tag{13.16}$$

and the normalized radiation amplitude pattern of the (matched) element or (matched) *element pattern* is

$$E_e(\theta) = \sqrt{\cos \theta} \tag{13.17}$$

For a given element spacing s, the total number of radiators N in the area A is $N = A/s^2$, and Eq. 13.16 gives

$$G_e(\theta) = 4\pi \left[\frac{s}{\lambda}\right]^2 \cos \theta$$

When the element spacing is $s = \lambda/2$, then the power pattern of an element that is perfectly matched at all scan angles is

$$G_e(\theta) = \pi \cos \theta \tag{13.18}$$

And the peak antenna gain in the direction of scan, θ_0, is

$$G(\theta_0) = \pi N \eta \cos \theta_0 \tag{13.19}$$

where the efficiency term η accounts for losses and for a nonuniform aperture distribution. For a broadside beam $\theta_0 = 0$ and

$$G_0 = \pi N \eta \tag{13.20}$$

and the element gain is $G_e = \pi$.

Figure 13.7 shows a theoretical example of the array and element factors and the resulting pattern for a 10-element array, with element spacing $s = \lambda/2$, scanned to 60°.

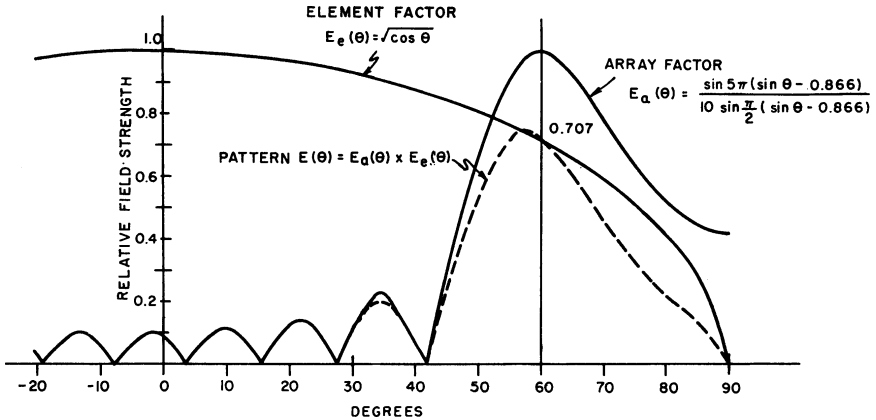

FIGURE 13.7 Ten-element linear array scanned to 60°; element spacing $s = \lambda/2$

The pattern maximum is noted to occur at less than 60° because the gain of the element pattern increases toward broadside. The element pattern value at 60° is cos 60° = 0.5 in power or 0.707 in amplitude, relative to the maximum at broadside, as expected. The sidelobes in the general region of broadside are not reduced because in that region the element pattern is approximately unity. Relative to the beam maximum, therefore, the sidelobes near broadside are increased by approximately 3 dB.

13.3 PLANAR ARRAYS AND BEAM STEERING

Planar Arrays. A planar array is capable of steering the beam in two dimensions. In a spherical-coordinate system, the two coordinates θ and ϕ define points on the surface of a unit hemisphere. As shown in Figure 13.8, θ is the angle of scan measured from broadside and ϕ is the plane of scan measured from the x axis. Von Aulock[43] has presented a simplified method for visualizing the patterns and the effect of scanning. He considers the projection of the points on a hemisphere onto a plane (Figure 13.9): the axes of the plane are the direction cosines cos α_x, cos α_y. For any direction on the hemisphere, the direction cosines are

$$\cos\alpha_x = \sin\theta\cos\phi$$
$$\cos\alpha_y = \sin\theta\sin\phi$$

The direction of scan is indicated by the direction cosines cos α_{xs}, cos α_{ys}. Here the plane of scan is defined by the angle ϕ measured counterclockwise from the cos α_x axis and is given by

$$\phi = \tan^{-1}\frac{\cos\alpha_{ys}}{\cos\alpha_{xs}}$$

The angle of scan θ is determined by the distance of the point (cos α_{xs}, cos α_{ys}) from the origin. This distance is equal to sin θ. For this reason, a representation of this sort is called sin θ space. A feature of sin θ space is that the antenna pattern shape is invariant

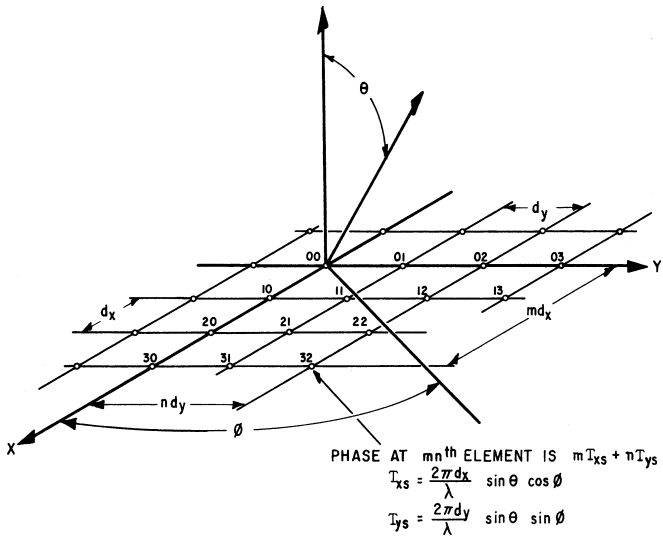

FIGURE 13.8 Planar-array-element geometry and phasing

to the direction of scan. As the beam is scanned, every point on the plot is translated in the same direction and by the same distance as is the beam maximum.

The region inside the unit circle where

$$\cos^2 \alpha_x + \cos^2 \alpha_y \leq 1$$

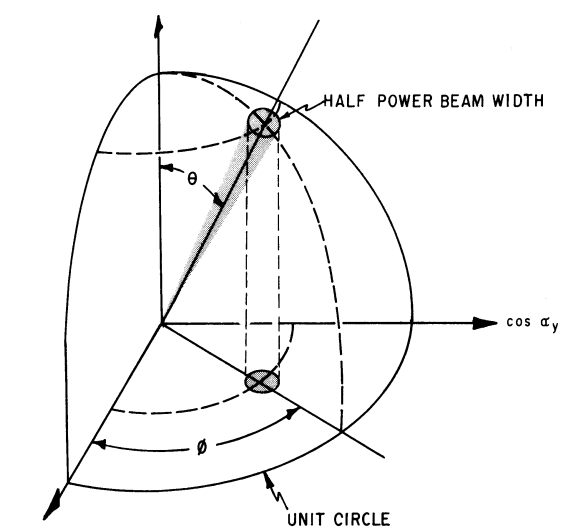

FIGURE 13.9 Projection of points on a hemisphere onto the plane of the array

is defined as *real space*, the hemisphere into which energy is radiated. The infinite region outside the unit circle is referred to as *imaginary space*. Although no power is radiated into imaginary space, the concept is useful for observing the motion of grating lobes as the array is scanned. In addition, the pattern in imaginary space represents stored energy and contributes to the element impedance in the array.

The most common element lattices have either a rectangular or a triangular grid. As shown in Figure 13.8, the *mn*th element is located at (md_x, nd_y). The triangular grid may be thought of as a rectangular grid where every other element has been omitted. The element locations can be defined by requiring that $m + n$ be even.

Calculations for the element-steering phases are greatly simplified by the adoption of the direction cosine coordinate system. In this system, the linear-phase tapers defined by the beam-steering direction ($\cos \alpha_{xs}$, $\cos \alpha_{ys}$) may be summed at each element so that the phasing at the *mn*th element is given by

$$\psi_{mn} = mT_{xs} + nT_{ys}$$

where $T_{xs} = (2\pi/\lambda)d_x \cos \alpha_{xs}$ = element-to-element phase shift in the x direction
$T_{ys} = (2\pi/\lambda)d_y \cos \alpha_{ys}$ = element-to-element phase shift in the y direction

The array factor of a two-dimensional array may be calculated by summing the vector contribution of each element in the array at each point in space. For an array scanned to a direction given by the direction cosines $\cos \alpha_{xs}$ and $\cos \alpha_{ys}$, the array factor of an $M \times N$ rectangular array of radiators may be written

$$E_a(\cos \alpha_{xs}, \cos \alpha_{ys}) = \sum_{m=0}^{M-1} \sum_{n=0}^{N-1} |A_{mn}| e^{j[m(T_x - T_{xs}) + n(T_y - T_{ys})]}$$

where $T_x = (2\pi/\lambda)\, d_x \cos \alpha_x$
$T_y = (2\pi/\lambda)\, d_y \cos \alpha_y$
A_{mn} = amplitude of *mn*th element

An array may be visualized as having an infinite number of grating lobes only one of which (namely, the main beam) is desired in real space. It is convenient to plot the position of the grating lobes when the beam is phased for broadside and observe the motion of these lobes as the beam is scanned. Figure 13.10 shows the grating-lobe locations for both rectangular and triangular spacing. For a rectangular array, the grating lobes are located at

$$\cos \alpha_{xs} - \cos \alpha_x = \pm \frac{\lambda}{d_x} p$$

$$\cos \alpha_{ys} - \cos \alpha_y = \pm \frac{\lambda}{d_y} q$$

$$p, q = 0, 1, 2, \ldots$$

The lobe at $p = q = 0$ is the main beam. A triangular grid is more efficient for suppressing grating lobes than a rectangular grid,[44] so that for a given aperture size,

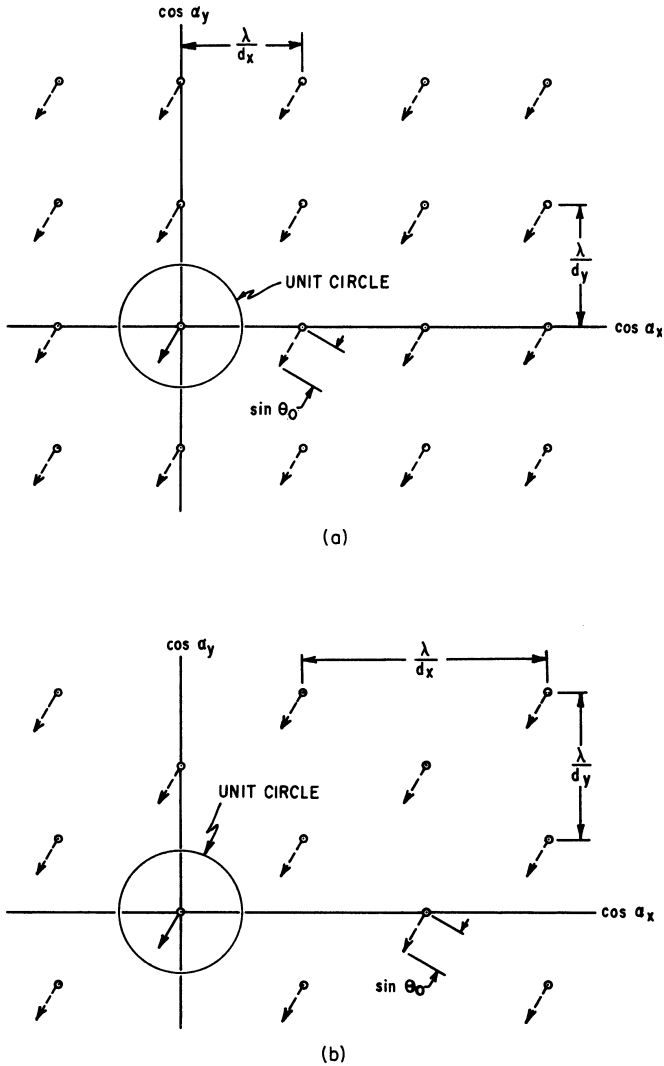

FIGURE 13.10 Grating-lobe positions for (*a*) rectangular and (*b*) triangular grids, showing the motion of the lobes as the beam is scanned at angle θ_0

fewer elements are required. If the triangular lattice contains elements at (md_x, nd_y), where $m + n$ is even, the grating lobes are located at

$$\cos \alpha_{xs} - \cos \alpha_x = \pm \frac{\lambda}{2d_x} p$$

$$\cos \alpha_{ys} - \cos \alpha_y = \pm \frac{\lambda}{2d_y} q$$

where $p + q$ is even.

Because only one main beam is normally desired in real space, an appropriate design will place all but one maximum in imaginary space for all angles of scan. With scanning, lobes that were originally in imaginary space may move into real space if the element spacing is greater than $\lambda/2$. As the array is scanned away from broadside, each grating lobe (in sin θ space) will move a distance equal to the sine of the angle of scan and in a direction determined by the plane of scan. To ensure that no grating lobes enter real space, the element spacing must be chosen so that for the maximum scan angle θ_m, the movement of a grating lobe by sin θ_m does not bring the grating lobe into real space. If a scan angle of 60° from broadside is required for every plane of scan, no grating lobes may exist within a circle of radius 1 + sin θ_m = 1.866. The square grid that meets this requirement has

$$\frac{\lambda}{d_x} = \frac{\lambda}{d_y} = 1.866 \quad \text{or} \quad d_x = d_y = 0.536\lambda$$

Here, the area per element is

$$d_x d_y = (0.536\lambda)^2 = 0.287\lambda^2$$

For an equilateral-triangular array, the requirement is satisfied by

$$\frac{\lambda}{d_y} = \frac{\lambda}{\sqrt{3}\, d_x} = 1.866 \quad \text{or} \quad d_y = 0.536\lambda \quad d_x = 0.309\lambda$$

Because elements are located only at every other value of *mn*, the area per element is

$$2d_x d_y = 2(0.536\lambda)(0.309\lambda) = 0.332\lambda^2$$

For the same amount of grating-lobe suppression, the square geometry requires approximately 16% more elements.

Element-Phasing Calculations. A computer is usually required to perform the steering computations for a phased array antenna. It can compensate for many of the known phase errors caused by the microwave components, the operating environment, and the physical placement of the elements. For example, if the insertion and differential phase variations (which may occur from phase shifter to phase shifter) are known, they may be taken into account in the computations. Known temperature variations across the array that would induce phase errors may be compensated for. Finally, many feeds (e.g., optical and series feeds) do not provide equal phase excitation at the input to each phase shifter. The relative phase excitation caused by these feeds is a known function of frequency. In these cases, the computer must provide a correction based on the location of the element in the array and on the frequency of operation.

For a large array with thousands of elements, many calculations are required to determine the phasing of the elements. These calculations must be performed in a short period of time. The use of the orthogonal phase commands mT_{xs}, nT_{ys} helps to minimize these calculations. Once the element-to-element phase increments T_{xs}, T_{ys} have been computed for a given beam-pointing direction, the integral multiples of T_{ys} may be used to steer the columns (Figure 13.8).

13.4 APERTURE MATCHING AND MUTUAL COUPLING[45]

Significance of Aperture Matching. An antenna is a device that acts as a transformer to provide a good match between a source of power and free space. If the antenna is not matched to free space, power will be reflected back toward the generator, resulting in a loss in radiated power. In addition, a mismatch produces standing waves on the feed line to the antenna. The voltage at the peaks of these standing waves is $(1 + |\Gamma|)$ times greater than the voltage of a matched line, where Γ is the voltage reflection coefficient. This corresponds to an increased power level that is $(1 + |\Gamma|)^2$ times as great as the actual incident power. Therefore, while the antenna is radiating less power, individual components must be designed to handle more peak power. With antennas that do not scan, the mismatch may often be tuned out by conventional techniques, preferably at a point as close to the source of the mismatch as possible.

In a scanning array, the impedance of a radiating element varies as the array is scanned, and the matching problem is considerably more complicated. Unlike a conventional antenna, where mismatch affects only the level of the power radiated and not the shape of the pattern, spurious lobes in the scanning array may appear as a consequence of the mismatch. Further, there are conditions where an antenna that is well matched at broadside may have some angle of scan at which most of the power is reflected.

The variation in element impedance and element pattern is a manifestation of the mutual coupling between radiating elements that are in close proximity to one another. For a practical design, two empirical techniques are of great value:

1. Waveguide simulators provide a means for determining the element impedance in an infinite array with the use of only a few elements. The effectiveness of a matching structure based on these measurements may also be determined in the simulator.
2. A small array is the best technique for determining the active element pattern. The active element pattern, obtained by exciting one element and terminating its neighbors, is the best overall measure of array performance other than the full array itself. If a large reflection occurs at some angle of scan, it can be recognized by a null in the element pattern. The small array can also provide data on the coupling between elements. This data can be used to calculate the variation in impedance as the array is scanned.

Both these techniques will be discussed later in this section.

Effects of Mutual Coupling. When two antennas (or elements) are widely separated, the energy coupled between them is small and the influence of one antenna on the current excitation and pattern of the other antenna is negligible. As the antennas are brought closer together, the coupling between them increases. In general, the magnitude of the coupling is influenced by the distance between the elements, the pattern of the elements, and the structure in the vicinity of the elements. For example, the radiation pattern of a dipole has a null in the $\theta = \pm 90°$ direction and is omnidirectional in the $\theta = 0°$ plane. Therefore, it can be expected that dipoles in line will be loosely coupled and parallel dipoles will be tightly coupled. When an element is placed in an array of many elements, the effects of coupling are sufficiently strong that the pattern and impedance of the elements in the array are drastically altered.

The terms *active element pattern* and *element impedance* refer to an element in its operating environment (i.e., in an array with its neighboring elements excited). In the array, each excited element couples to every other element. The coupling from several elements to a typical central element, element 00, is shown in Figure 13.11. The $C_{mn,pq}$ are mutual-coupling coefficients relating the voltage (amplitude and phase) induced in the *mn*th element to the voltage excitation at the *pq*th element. The coupled signals add vectorially to produce a wave traveling toward the generator of element 00 that appears to be a reflection from the radiator of element 00. As the phases of the neighboring elements are varied to scan the beam, the vector sum of the coupled signals changes and causes an apparent change in the impedance of element 00. For some scan angles, the coupled voltages tend to add in phase, causing a large reflection and possibly the loss of the main beam. Large reflections often occur at scan angles just prior to the emergence of a grating lobe into real space, but in some instances such reflections may occur at smaller scan angles.

The description of the impedance variation given above made no reference to the feed network or the phase shifters and assumed that the only coupling between elements is via the radiating aperture. The coupling coefficients would be measured, and by superposition, the phased-voltage contributions from every element in the array (or at least those in the immediate vicinity) would be added vectorially to produce the voltage reflected back toward the generator. In a practical array, the impedance variation depends upon the feed system and the phase shifter. If these are taken into account, the impedance variation may be different from what the above model might predict. In most analyses, only the coupling at the aperture is considered. This description provides insight into the intrinsic impedance variation of the aperture when it is isolated from other effects, as in the case where each element has an independent feed (e.g., its own generator and isolator). In this case it, is a simple matter to measure the voltage-standing-wave ratio (VSWR) in any line and determine exactly the extent of the impedance and mismatch variation. For many feed systems, this is not possible, and a measurement of the reflected energy will provide erroneous information and a

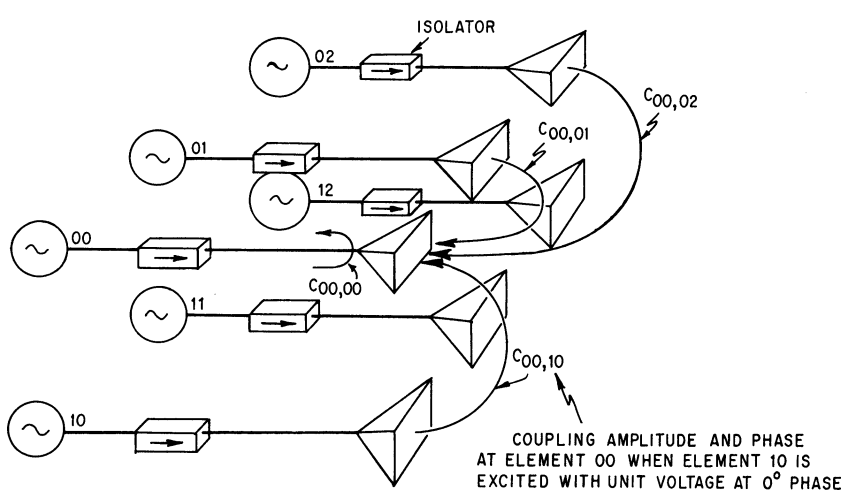

FIGURE 13.11 Coupled signals to a central element from neighboring elements

false sense of security. Unless all the reflections are collimated back at some central point (or independent feeds are used), some of the reflected energy will generally be re-reflected and contribute to undesirable sidelobes.

For large arrays, the impedance of an element located near the center of the array is often taken as typical of the impedance of every element in the array. As might be expected, this element is most strongly influenced by elements in its immediate vicinity. When the array is scanned, the influence of elements several wavelengths distant is also significant. For dipoles above a ground plane, the magnitude of the coupling between elements decays rapidly with distance. For a reasonable indication of array performance, an element in the center of a 5-by-5 array may be taken as typical of an element in a large array. For dipoles with no ground plane the coupling between elements does not decay so rapidly, and a 9-by-9 array appears reasonable. For an array of open-ended waveguides, a 7-by-7 array should suffice. If accurate prediction of the array performance is required, many more elements are needed than are indicated above.[47,48]

It is often convenient to assume that the array is infinite in extent and has a uniform amplitude distribution and a linear-phase taper from element to element. In this manner, every element in the array sees exactly the same environment, and the calculations for any element apply equally to all. These assumptions provide a significant simplification in the calculation of the element impedance variations. In addition, impedance measurements made in simulators correspond to the element impedance in an infinite array. In spite of the assumptions, the infinite-array model has predicted with good accuracy the array impedance and the impedance variations. Even arrays of modest proportions (less than 100 elements) have been in reasonable agreement with the results predicted for an infinite array.[49]

Element Pattern. From energy considerations, the directional gain of a perfectly matched array with constant amplitude distribution ($\eta = 1$) will vary as the projected aperture area from Eq. 13.14:

$$G(\theta_0) = \frac{4\pi A}{\lambda^2} \cos \theta_0$$

If it is assumed that each of the N elements in the array shares the gain equally, the gain of a single element is from Eq. 13.16:

$$G_e(\theta) = \frac{4\pi A}{N\lambda^2} \cos \theta_0$$

If the element is mismatched, having a reflection coefficient $\Gamma(\theta, \phi)$ that varies as a function of scan angle, the element gain pattern is reduced to

$$G_e(\theta) = \frac{4\pi A}{N\lambda^2} (\cos \theta)[1 - |\Gamma(\theta, \phi)|^2]$$

The element pattern is seen to contain information pertaining to the element impedance.[50–53] The difference between the total power radiated in the element pattern and the power delivered to the antenna terminals must equal the reflected power. In terms of the radiation pattern of the scanning array, this means that since the scanned antenna patterns trace out the element pattern, it follows that the average power lost from the scanned pattern is equal to the power lost from the element

pattern because of reflections. It is not enough to match one element in the presence of all its terminated neighbors. The element will deliver power to its neighbors, and this loss in power corresponds to the average power lost when scanning. An ideal, although not necessarily realizable element pattern, would place all the radiated power into the scan region, giving a pattern like a cosine on a pedestal and thereby providing maximum antenna gain for the number of elements used.

Thinned Arrays. The number of radiating elements in an array may be reduced to a fraction of those needed completely to fill the aperture without suffering serious degradation in the shape of the main beam. However, average sidelobes are degraded in proportion to the number of elements removed. The element density may be thinned so as to taper the amplitude distribution effectively, and the spacing is such that no coherent addition can occur to form grating lobes. A thinned aperture, where elements have been removed randomly from a regular grid,[54] is shown in Figure 13.12. The gain is that due to the actual number of elements $NG_e(\theta)$, but the beamwidth is that

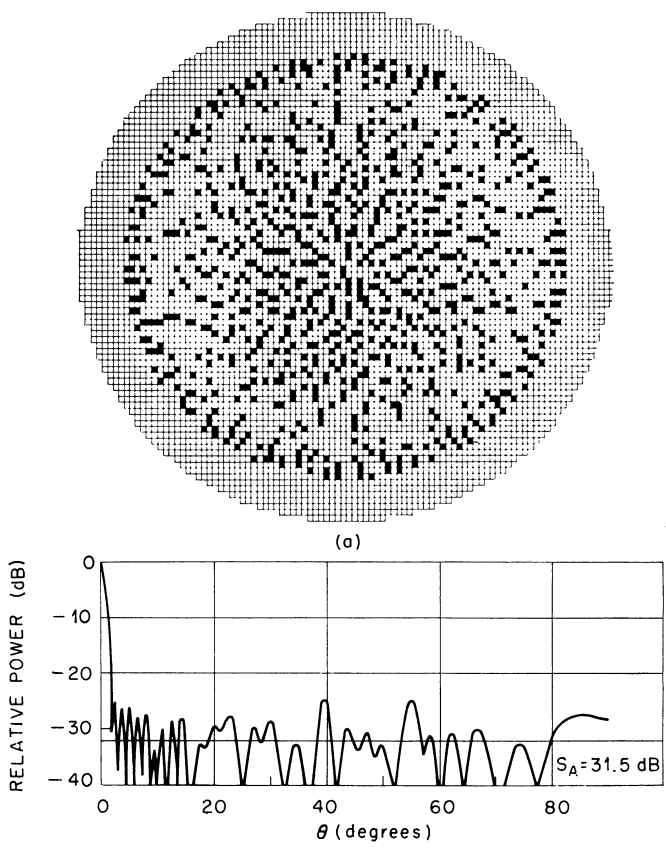

FIGURE 13.12 (*a*) Thinned array with a 4000-element grid containing 900 elements. (*b*) Pattern for a thinned array. S_A is the average sidelobe level. (*after R. E. Willey*[54] *© IRE 1962. Courtesy of Bendix Radio.*)

of the full aperture. For example, if the array has been thinned so that only 10% of the elements are used, the gain of the array will drop by 10 dB. However, because the main beam is virtually unchanged, about 90% of the power is delivered to the sidelobe region. Thinned arrays are seldom used.

If the removed elements (in a regular thinned array) are replaced with elements with matched loads, the element pattern is identical to that of one in the regular array with all elements excited. The element pattern is independent of the array excitation, and the same fractional amount of power will be lost (because of mismatch) whether the array is thinned, tapered, or uniformly illuminated. It should be noted that the concept of an element pattern that applies equally to every element is valid only when isolating feeds are used and edge effects are ignored.

A thinned array may also be implemented with an irregular element spacing, although this is not common. In this case, the element gain (and impedance) will vary from element, depending upon the environment of a given element. To obtain the gain of the array, it is necessary to sum all the different element gains $G_{en}(\theta)$. Thus

$$G(\theta) = \sum_n G_{en}(\theta)$$

Impedance Variation of Free Space. It is of interest to examine the case of a large continuous aperture that may be considered to be the limiting case of an array of many very small elements.[55] The free-space impedance E/H varies as cos θ for scanning in the E plane and as sec θ for scanning in the H plane. The impedance of a medium is thus dependent upon the direction of propagation, and the impedance variation of a scanning aperture is a natural consequence of this dependence. The continuous aperture appears to represent a lower limit to the impedance variation with scanning. This is indicated by Allen's results[56] where impedance variation with scanning was calculated for dipoles above a ground plane. In spite of increased mutual coupling, or perhaps because of it, the more closely the dipoles were spaced, the smaller the impedance variation with scanning. Although the impedance variation decreased, the absolute impedance of the dipoles also decreased, making them more difficult to match at broadside. It is expected that to obtain an impedance variation smaller than that of free space some impedance compensation must be employed.

Mutual Coupling and Surface Waves. The mutual coupling between two small isolated dipoles[57] should decrease as $1/r$ in the H plane and $1/r^2$ in the E plane (E and H planes are interchanged for slots). Coupling measurements[58] have shown that in the array environment the rate of decay is slightly greater than predicted above, indicating that some of the energy is delivered to other elements in the array and may be dissipated and reradiated from these elements. The same measurements have shown that the phase difference of the energy coupled to elements is directly proportional to their distance from the excited elements, indicative of a surface wave traveling along the array, leaking energy to each of the elements. For best performance, the velocity of the surface wave should be very close to that of free space. If the array contains waveguides or horns loaded with dielectric, the velocity will decrease slightly. Further, if the dielectric protrudes from the radiators or if a dielectric sheet is used in front of the array, the velocity of the surface wave may decrease dramatically. This surface wave is important because it can cause a large reflection (and an accompanying loss of the beam) for some angles of scan. This can best be seen by examining the condition of

phasing for which the couplings from many elements will add in-phase to cause a large reflection in a typical element.

Consider an array in which the velocity of the surface wave is that of free space. The difference in the phase of the voltages coupled from an adjacent pair of elements to element 00 (e_{00} in Figure 13.13) is related to the scan angle by

$$\frac{2\pi s}{\lambda} + \frac{2\pi s}{\lambda} \sin \theta_0 = \frac{2\pi s}{\lambda}(1 + \sin \theta_0)$$

The couplings will be in phase when $\Delta\psi = 2\pi$ or when

$$\frac{s}{\lambda} = \frac{1}{1 + \sin \theta_0}$$

This is seen to be exactly the same conditions as previously determined for the emergence of a grating lobe into real space. Therefore, it may be expected that when a grating lobe is about to emerge into real space, the coupled voltages tend to add in phase and cause a large mismatch.

Array Simulators. A good deal of effort has gone into matching a radiator in the presence of an array of radiators. The use of waveguide simulators as developed by Wheeler Laboratories has made it possible to determine the matching structure experimentally without needing to build an array. A waveguide, operating in a TE_{10} mode, may be considered to contain two inclined–plane waves propagating down the guide. The angle that each of the plane waves makes with the longitudinal direction (Figure 13.14) is determined by the H dimension of the waveguide and simulates the angle of scan of an infinite array

$$\sin \theta = \frac{\lambda}{\lambda_c} \tag{13.21}$$

where θ = scan angle
λ = free-space wavelength
λ_c = cutoff wavelength of guide

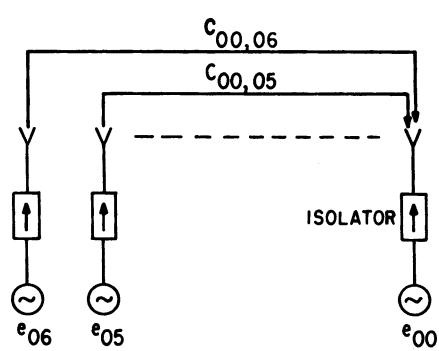

FIGURE 13.13 Two adjacent elements coupling to another element in the same row

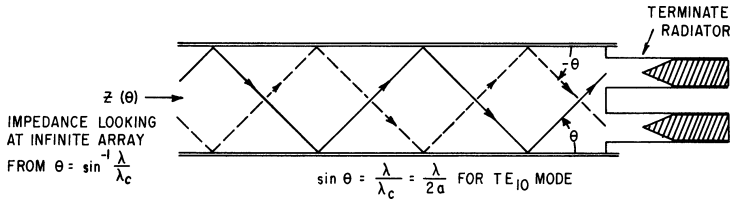

FIGURE 13.14 Array simulator terminated with two dummy elements

Additional scan angles may be simulated by exciting other modes. The waveguide dimensions are chosen so that a radiating element or element placed in the waveguide sees mirror images in the walls of the waveguide that appear to be at the same spacing as the array to be simulated. Both rectangular and triangular arrays may be simulated, as shown in Figure 13.15. The impedance measurements are made by looking into a waveguide simulator that is terminated with dummy elements. This is equivalent to looking at an infinite array from free space at a scan angle given by Eq. 13.21. A matching structure, designed from the simulator impedance data, may be placed into the simulator to measure its effectiveness. Several simulator designs, results, and a complete discussion of the topic have been presented by Hannan and Balfour.[59] The technique is limited in that only discrete scan angles can be simulated. Several scan angles in both planes of scan give a general idea of the array impedance.

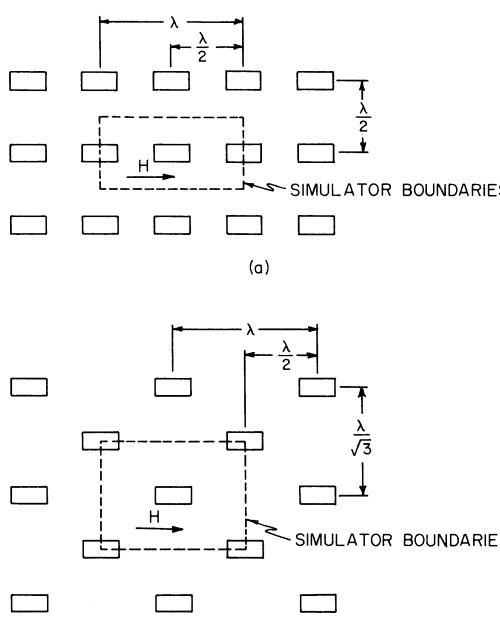

FIGURE 13.15 Rectangular- and triangular-array geometries with simulator boundaries superimposed: (*a*) square array with simulator superimposed and (*b*) triangular array with simulator superimposed

Compensation for Scanned Impedance Variation. The impedance of an element in an array has been discussed and has been shown to vary as the array is scanned. An array that is matched at broadside can be expected to have at least a 2:1 VSWR at a 60° angle of scan. To compensate for the impedance variation, it is necessary to have a compensation network that is also dependent on scanning.

Small Arrays. The element pattern is the best single indicator of impedance matching in a scanning array. One way of determining the element pattern is to build a small array. A central element is excited, and all other elements are terminated. The pattern of this central element is the active element pattern. Diamond[60] has examined the number of elements required in a small array to provide a reasonable approximation to an element in an infinite array. He concludes that 25 to 37 elements are required to provide a good indication. Figure 13.16 shows the change in the measured active element pattern as the number of elements is increased. For a 41-element array, the null is very pronounced. Even for the 23-element array, it is clear that the gain variation with scanning is dramatically greater than cos θ.

The small array can also be used to measure coupling coefficients as demonstrated by Figure 13.11 These coupling coefficients can be used to calculate the impedance variation as the array is scanned. Grove, Martin, and Pepe[61] have noted that for the element to be matched in its operating environment the self-coupling must exactly cancel the coupling from all other elements. They have used this technique to provide a good match on an ultralow-sidelobe wideband phased array.

The combination of waveguide simulators and small arrays provides powerful empirical tools to supplement the analytical techniques. Experience has demonstrated that a large antenna should not be built until the element pattern has been verified with a small array.

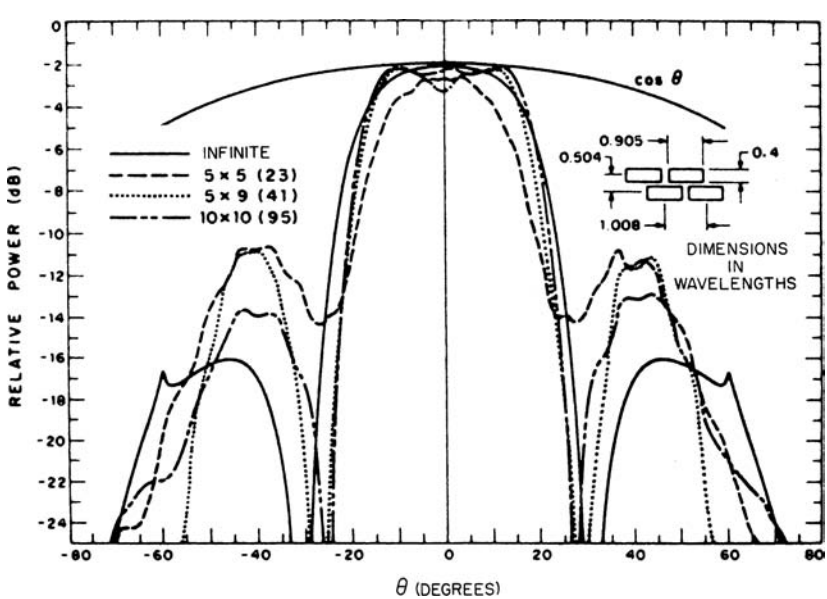

FIGURE 13.16 Experimental H-plane patterns of the center elements of waveguides arrays (*after B. L. Diamond*[60] *© Artech House 1972*)

13.5 LOW-SIDELOBE PHASED ARRAYS

Low sidelobes have long been of interest to antenna designers. This interest has been heightened by the jamming that threatens most military radars. The requirement for low sidelobes for clutter rejection in the AWACS radar resulted in technology that now supports sidelobe levels of more than 50 dB below the main-beam peak.[62,63] The price that must be paid to achieve these low sidelobes includes (1) a reduction in gain, (2) an increase in beamwidth, (3) increased tolerance control, (4) increased cost, and (5) the need to operate in an environment free from obstructions that can readily increase the sidelobes.[64] In spite of these drawbacks, the trend to low-sidelobe antennas has accelerated since low sidelobes provide a counter to electronic countermeasures (ECM).

Antenna sidelobes can be controlled by the aperture amplitude distribution. For phased arrays, the amplitude of each element may be controlled individually, and therefore, good sidelobe control can be achieved. The process of designing a low-sidelobe antenna can be considered in two parts:

1. Choose the correct illumination function to achieve the desired design (error-free) sidelobes.
2. Control the phase and amplitude errors that contribute to the random sidelobes.

Of the two, controlling errors fundamentally limits sidelobe performance. The effects of illumination function and errors are discussed below.

Illumination Functions. The relation between aperture illumination and the far-field pattern has been studied extensively and is well documented in the literature.[65–68] For a continuous aperture, the far-field pattern is the Fourier transform of the distribution across the aperture. For an array, samples are taken of the continuous distribution at each of the discrete locations. Some typical illumination functions are given in Table 13.1. It is seen that uniform illumination (constant amplitude) results in the highest gain and the narrowest beamwidth but at the cost of high sidelobes. As the amplitude is tapered, the gain drops, the beam broadens, and the sidelobes may be reduced. It is important for the antenna designer to choose an efficient and realizable illumination function that provides low sidelobes at a minimum loss in gain. For low-sidelobe radars, the Taylor illumination[69,70] for the sum patterns and the Bayliss illumination[71] for the difference patterns have almost become an industry standard. The Taylor illumination is somewhat similar to a cosine squared on a pedestal and is readily implemented. The Bayliss illumination is a derivative form of the Taylor illumination and is also readily implemented. It should be noted that in many phased arrays the sidelobe performance for the difference pattern is comparable to that of the sum pattern. For both sum and difference patterns, the sidelobes are referenced to the peak of the sum pattern. The beamwidth factor provides the beamwidth, in degrees, of an aperture with length a.

Figure 13.17 gives the approximate loss in gain and the beamwidth factor for the Taylor illumination as the sidelobes change. For a more comprehensive treatment, see Barton and Ward.[72] The sidelobes predicted by Table 13.1 are for antennas that have perfect phase and amplitude across the aperture. To allow for errors, aperture illuminations are often chosen to provide peak sidelobes below those required. For example, if the antenna specification calls for –40 dB sidelobes, a Taylor illumination that provides –45 dB design sidelobes might be chosen. The terminology $\bar{n}$ indicates that the first n sidelobes are held to the specified level.

TABLE 13.1 Illumination Functions

Illumination Function	Efficiency, η	Peak Sidelobe, dB	Beamwidth Factor, k
Linear illumination functions: beamwidth = $k\lambda/a$ (degrees); a = length of antenna			
Uniform	1	−13.3	50.8
Cosine	0.81	−23	68.2
Cosine square (Hanning)	0.67	−32	82.5
Cosine squared on 10 dB pedestal	0.88	−26	62
Cosine square on 20 dB pedestal	0.75	−40	73.5
Hamming	0.73	−43	74.2
Taylor $\bar{n} = 3$	0.9	−26	60.1
Taylor $\bar{n} = 5$	0.8	−36	67.5
Taylor $\bar{n} = 8$	0.73	−46	74.5
Circular illumination functions: beamwidth = $k\lambda/D$ (degrees); D = diameter of antenna			
Uniform	1	−17.6	58.2
Taylor $\bar{n} = 3$	0.91	−26.2	64.2
Taylor $\bar{n} = 5$	0.77	−36.6	70.7
Taylor $\bar{n} = 8$	0.65	−45	76.4

It should be noted that for a rectangular array a different illumination may be chosen for each plane. This is appropriate if the sidelobe requirements in each of the planes are different. The resultant loss in gain is then the sum (in decibels) of the losses in each plane.

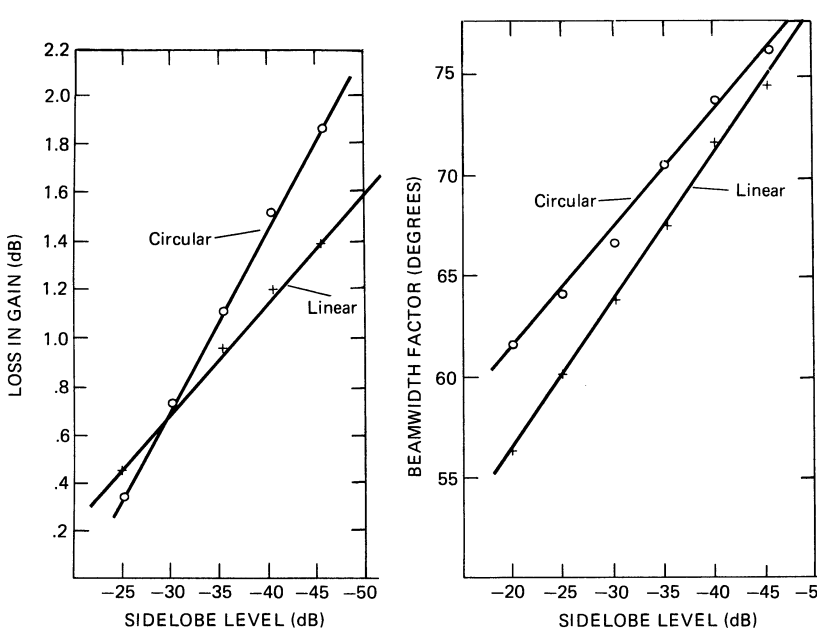

FIGURE 13.17 Taylor illumination: loss and beamwidth factor

Effect of Errors. When errors occur in phase or amplitude, energy is removed from the main beam and distributed to the sidelobes. If the errors are purely random, they create random sidelobes that are considered to be radiated with the gain and pattern of the element. When the errors are correlated, the sidelobe energy will be lumped at discrete locations in the far field. The correlated errors will, therefore, provide higher sidelobes, but only at a limited number of locations. Both correlated and random sidelobes are of concern to antenna designers. Correlated errors are discussed in Section 13.6.

Analyses of the far-field effect of errors are based on the fact that antennas are linear devices. That is, the far-field pattern is the sum of the voltage (amplitude and phase) of each radiating element in the antenna. For this reason, the far-field voltage pattern can be considered to be the sum of the design pattern plus the pattern created solely by the errors:

$$E_T(\theta,\phi) = E_{\text{design}}(\theta,\phi) + E_{\text{error}}(\theta,\phi)$$

In general, three regions will be recognized in the total resultant pattern: a low noise floor generated by random errors that follow the element pattern, a few peak sidelobes due to correlated errors, and the main beam with its sidelobes due to the design distribution.

Random Errors. Allen[73] and Ruze[74] have made detailed analyses of the effects of random errors on antennas. This discussion will follow the analysis performed by Allen. As previously mentioned, amplitude and phase errors take a fraction of the energy from the main beam and distribute this energy to the sidelobes. This fraction is, for small independent random errors,

$$\sigma_T^2 = \sigma_\phi^2 + \sigma_A^2$$

where σ_ϕ = rms phase error, rad
σ_A = rms amplitude error, volts/volt (V/V)

This energy is radiated into the far field with the gain of the element pattern. To determine the mean-squared-sidelobe level (MSSL), it is necessary to compare this energy with the peak of the pattern of an array of N elements so that the mean-squared-sidelobe level is

$$\text{MSSL} = \frac{\sigma_T^2}{\eta_a N(1-\sigma_T^2)} \tag{13.22}$$

Note that in the denominator of this expression the gain due to the array factor N is reduced by the aperture efficiency η_a and by the error power lost from the main beam $(1-\sigma_T^2)$. As an example, consider an array of 5000 elements with an aperture efficiency of 70%, $\sigma_a = 0.1$ v/v, and $\sigma_\phi = 0.1$ rad. Then $\sigma_T^2 = (0.1)^2 + (0.1)^2 = 0.02$.

$$\text{MSSL} = \frac{\sigma_T^2}{\eta N(1-\sigma_T^2)} = \frac{0.02}{(0.7)(5000)(0.98)} = 5.8 \times 10^{-6} = -52 \text{ dB}$$

The result is that this array has a mean floor of random sidelobes that on the average is 52 dB below the peak of the beam. It also illustrates that to achieve low sidelobes

very tight tolerances are required. The amplitude of 0.1 v/v is equivalent to a total amplitude standard deviation of 0.83 dB rms. The total rms phase error is 5.7°. It should be noted that there are numerous sources of phase and amplitude errors that are induced by the phase shifters, the feed network, the radiating elements, and the mechanical structure. The task of building a low-sidelobe antenna is one of reducing each of the amplitude errors to a few tenths of a decibel and the phase errors to a few degrees. The fewer the number of elements used, the tighter the tolerance becomes.

The individual effects of phase and amplitude errors and failed elements are summarized in Figure 13.18.[75] The resultant rms sidelobes are referenced to the gain of a single element so that the curve can be used for any number of elements with independent errors. For example, a 5° rms phase error will produce an rms sidelobe level that is approximately 21 dB below the gain of an element. If 1000 elements (30 dB) are used, the rms sidelobe level is 51 dB below the gain of the array. This is the effect of only the random phase errors. The effects due to amplitude errors and failed elements must also be included.

The previous discussion applies to the rms sidelobe level. This analysis has been extended by Allen[73] to apply the probability of keeping a single sidelobe below a given

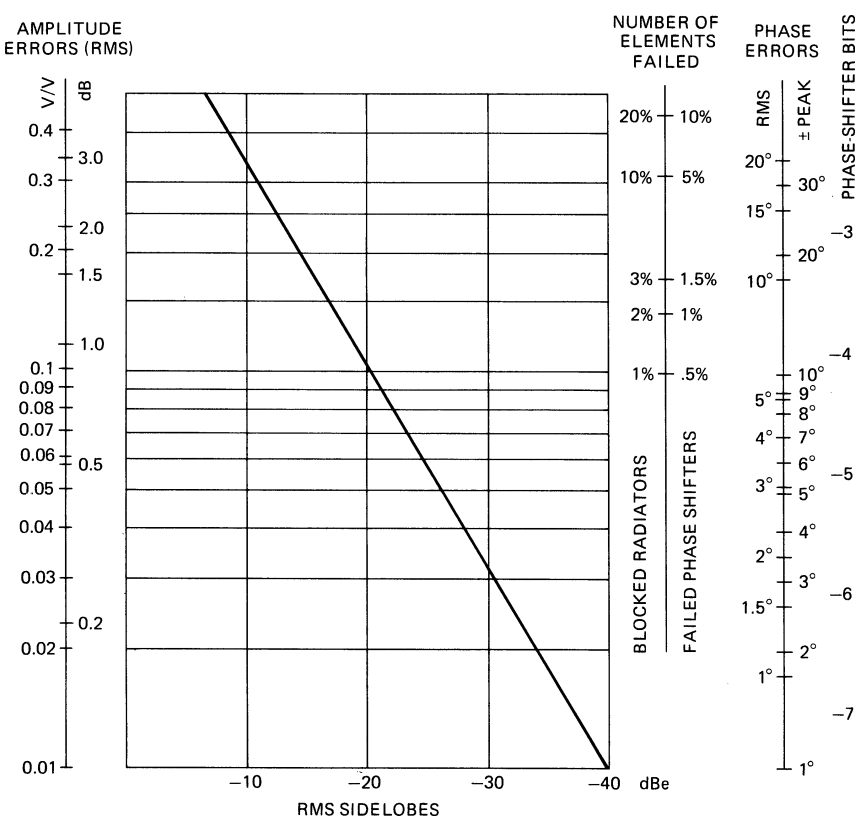

FIGURE 13.18 Random errors and rms sidelobes

level and then the probability of keeping a number of sidelobes below a given level. By ignoring the element pattern, the MSSL including failed elements is given by

$$\text{MSSL} = \frac{(1-P) + \sigma_A^2 + P\sigma_\phi^2}{\eta_a PN}$$

where $1 - P$ = probability of a failed element. Note that if $P = 1$ (no failed elements), this equation becomes

$$\text{MSSL} = \frac{\sigma_A^2 + \sigma_\phi^2}{\eta_a N} = \frac{\sigma_T^2}{\eta_a N}$$

This is the same as Eq. 13.22 except for $(1-\sigma_T^2)$ in the denominator, which is not significant for low-sidelobe antennas. For the case in which the design sidelobes are well below the sidelobes caused by errors, Allen has developed the set of curves shown in Figure 13.19. An example will illustrate the use of these curves. If you desire to hold the sidelobe at a given point in space to less than 40 dB below the peak of the beam with a probability of 0.99, draw a vertical line from –40 dB on the abscissa until it intersects the 0.99 curve. From this intersection, draw a horizontal line and read the value of MSSL, in this case –47 dB. Then

$$\text{MSSL} = -47 \text{ dB}$$

or

$$\text{MSSL} = 2 \times 10^{-5} = \frac{(1-P) + \sigma_A^2 + P\sigma_\phi^2}{\eta_a PN}$$

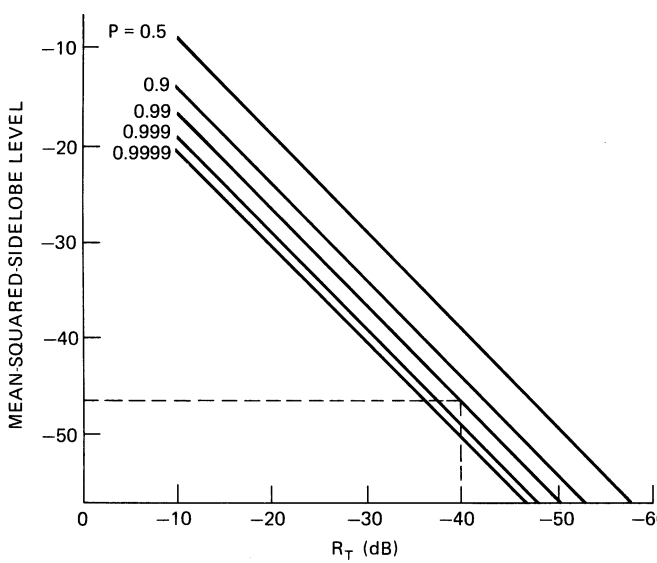

FIGURE 13.19 Sidelobe level to be held with probability P (*after J. L. Allen*[73])

For a 10,000-element array,

$$0.2 = \frac{(1-P) + \sigma_A^2 + P\sigma_\phi^2}{\eta_a P}$$

For $\eta_a = 1$, this array can tolerate $P = 0.83$, or $\sigma_A = 3.2$ dB, or $\sigma_\phi = 25.6°$. Naturally, each type of error must be anticipated, and one must allow a budget for failed elements, amplitude errors, and phase errors.

For a number of independent sidelobes, the probability that n sidelobes can be kept below a given level R_T is equal to the product of the probabilities that each sidelobe can be held below this level:

$$P\,[n \text{ sidelobes} < R_T] = \prod_{i=1}^{n} P[R(\theta_i) < R_T]$$

$$R(\theta_i) = \text{sidelobe level at } \theta_i$$

Assuming the same sidelobe requirement at each θ_i,

$$P\,[n \text{ sidelobes} < R_T] = \{1 - P\,[\text{one sidelobe} > R_T]\}^n$$

and for $P\,[\text{one sidelobe} > R_T] \ll 1$,

$$P\,[n \text{ sidelobes} < R_T] \cong 1 - n\,P\,[\text{one sidelobe} > R_T]$$

A simple example will illustrate the process. If it is necessary to keep all 100 sidelobes in a sector below –40 dB with a probability of 0.9, determine the required probability on any one given sidelobe:

$$0.9 = P\,[100 \text{ sidelobes} < 40 \text{ dB}]$$

Then

$$0.9 = 1 - 100\,P\,[\text{one given sidelobe} > 40 \text{ dB}]$$

$$0.001 = P\,[\text{one given sidelobe} > 40 \text{ dB}]$$

$$0.999 = P\,[\text{one given sidelobe} < 40 \text{ dB}]$$

That is, to keep all 100 sidelobes below –40 dB with a probability of 0.9, it is necessary to keep any given sidelobe below –40 dB with a probability of 0.999. The process of controlling each and every sidelobe is thus seen as formidable, since the total number of sidelobes is approximately equal to the number of elements in a phased array. For a 5000-element array and a probability of 0.999 that a single sidelobe will not exceed R_T at any single location, it will still be expected that 5 sidelobes will exceed R_T when all 5000 sidelobe locations are taken into account.

For very low sidelobe arrays, it is reasonable to allow a few sidelobes to exceed the MSSL value by as much as 10 to 12 dB to account for random variations. This can be seen from Figure 13.19 as the difference between $P = 0.5$ and $P = 0.999$ or $P = 0.9999$. If this allowance is not granted, the antenna will be overdesigned. It is worthwhile to do some probability calculations before specifying the exact sidelobe requirements.

13.6 QUANTIZATION EFFECTS

Of concern here are errors peculiar to phased arrays, which are due to the quantization of amplitude and phase and to the lobes that occur when these errors are repeated periodically. The effect on the gain and radiation pattern of random errors in the antenna excitation function is discussed in Section 13.5.

Phase Quantization. Phase shifters suitable for steering phased arrays are described in Section 13.9. Most of these phase shifters are digitally controlled and can be set with an accuracy that is a function of the number of bits. A small number of bits is desired for simplicity of phase-shift computation and operation, for minimal insertion loss in the case of diode phase shifters, and for minimal cost. On the other hand, a large number of bits is required for best performance in terms of gain, sidelobes, and beam-pointing accuracy.

Phase Errors. The phase of a phase shifter having P bits can be set to the desired value with a residual error:

$$\text{Peak phase error} = \alpha = \pm\frac{\pi}{2^P} \tag{13.23}$$

$$\text{RMS phase error} = \sigma_\phi = \frac{\pi}{2^P\sqrt{3}} \tag{13.24}$$

Loss in Gain. As discussed in Section 13.5, the loss in gain is $\sigma_\phi{}^2$, which with Eq. 13.24 gives

$$\Delta G \approx \sigma_\phi{}^2 = \frac{1}{3}\frac{\pi^2}{2^{2P}} \tag{13.25}$$

With many array elements, this result is statistically independent of the amplitude distribution. An enumeration of Eq. 13.25 gives

Number of phase-shifter bits, P	2	3	4
Loss in gain ΔG, dB	1.0	0.23	0.06

From the point of view of gain, therefore, 3 or 4 bits would appear ample.

RMS Sidelobes. Phase quantization decreases the gain of the main beam, as shown above. The energy that has been lost is distributed to the sidelobes. The resulting rms sidelobes are, therefore, σ_ϕ^2 relative to the gain of a single element, as shown in Figure 13.18.

Beam-Pointing Accuracy. The accurate determination of the direction of targets is made with the monopulse difference pattern. The accuracy of the null position of the difference pattern is, therefore, of interest. With quantized phase shifters, the position of this null can be moved with a granularity that is a function of the bit size.

Following the analysis of Frank and Ruze,[76] Figure 13.20 shows an aperture with an even number of elements N, separated by distances s. All elements are excited with

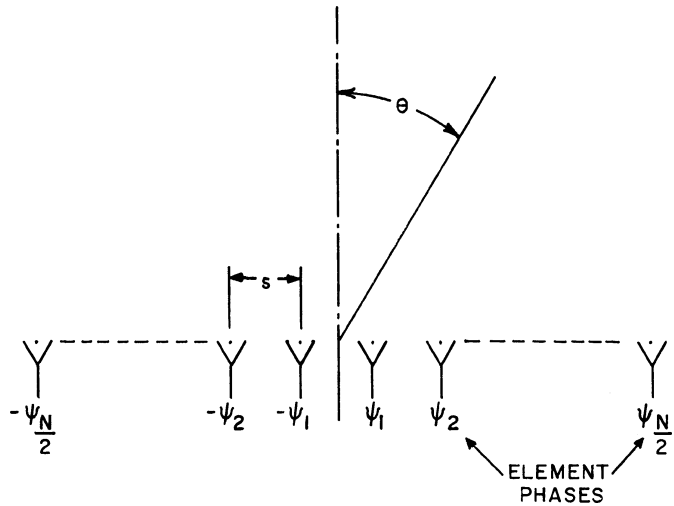

FIGURE 13.20 Antisymmetrically phased array

equal amplitude and antisymmetric phase to give a difference pattern. The steering increment is shown to be

$$\delta\theta = \frac{9}{N2^P}\theta_B(\text{scanned})$$

Periodic Errors

Periodic Amplitude and Phase Modulation. Both amplitude and phase quantization lead to discontinuities that may be periodic and give rise to *quantization lobes* that are similar to grating lobes.

Amplitude or phase errors that vary cosinusoidally may be analyzed simply after Brown.[77] Figure 13.21*a* shows an original amplitude distribution $F(x)$ disturbed by a cosinusoidal ripple $q \cos(2\pi x/s)$, giving a new distribution $F'(x)$ such that

$$F'(x) = F(x) + qF(x)\cos\frac{2\pi x}{s}$$

$$= F(x) + \frac{q}{2}\left[F(x)e^{j(2\pi x/s)} + F(x)e^{-j(2\pi x/s)}\right]$$

When the beam is scanned to θ_0, the quantization lobes occur at an angle θ_1, where

$$\sin\theta_1 = \sin\theta_0 \pm \frac{1}{s/\lambda}$$

The gain of the aperture varies as $\cos\theta$, and the relative amplitude of the quantization lobe is modified by the factor $\sqrt{(\cos\theta_1)/(\cos\theta_0)}$. Figure 13.21*b–g* shows the effects of various other periodic aperture modulations.

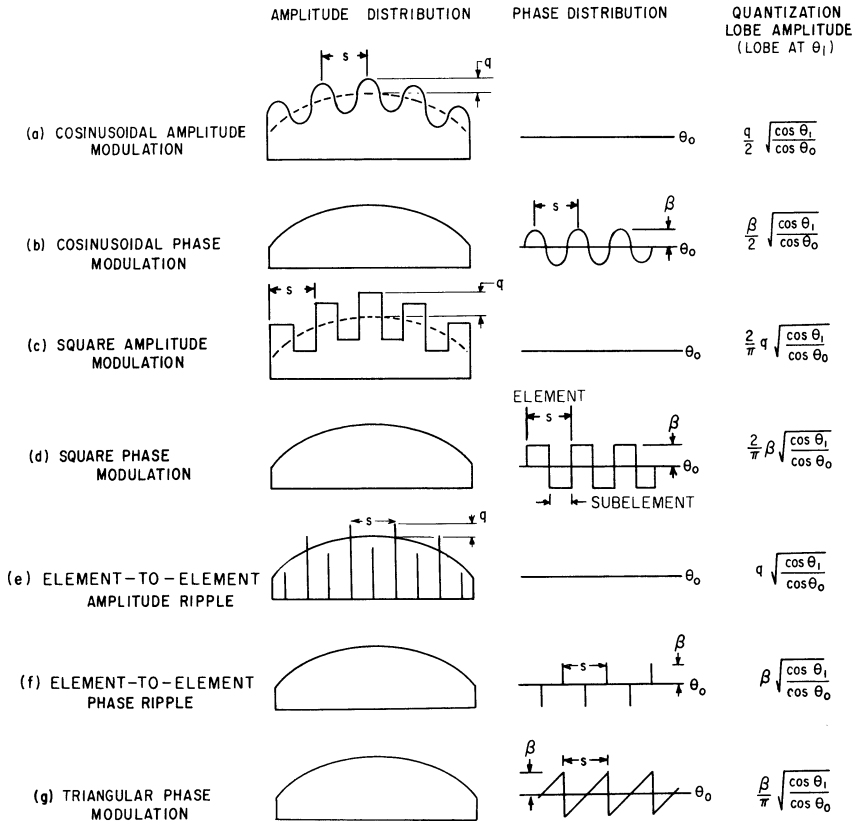

FIGURE 13.21 Effects of periodic amplitude and phase modulation ($\sin\theta_1 = \sin\theta_0 \pm \lambda/s$)

Phase-Shifter Quantization Lobes. Peak quantization sidelobe values are derived by Miller[78] considering the actual aperture phase distribution. Figure 13.22 shows this distribution for some scan angle θ_0 and the resulting errors due to phase quantization. Although a continuous curve has been drawn, only points corresponding to integral values of M are meaningful.

The greatest phase-quantization lobes seem to occur with a phase slope such that the elements are spaced by a distance exactly one-half of the period or an exact odd multiple thereof. The phase error under this condition has element-to-element phase ripples with a peak-to-peak value of $\alpha = \pi/2^p$. The value of the peak phase-quantization lobes for the case shown in Figures 13.21*f* and 13.22 are given in Figure 13.23. An examination of Figure 13.23 shows that peak phase-quantization lobes are significant and attempts should be made to reduce them.

Reduction of Peak Phase-Quantization Lobes. Miller[78] points out that peak quantization lobes can be reduced by decorrelating the phase-quantization errors. This may be done by adding a constant phase shift in the path to each radiator, with a value that differs from radiator to radiator by amounts that are unrelated to the bit size.

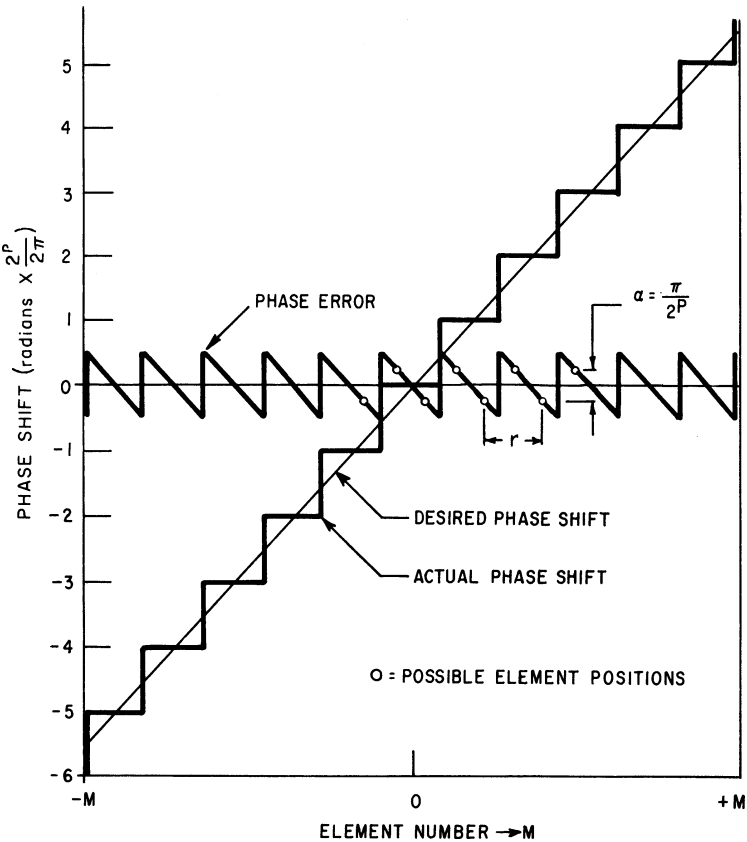

FIGURE 13.22 Aperture phase error due to phase quantization (*from Miller*[78])

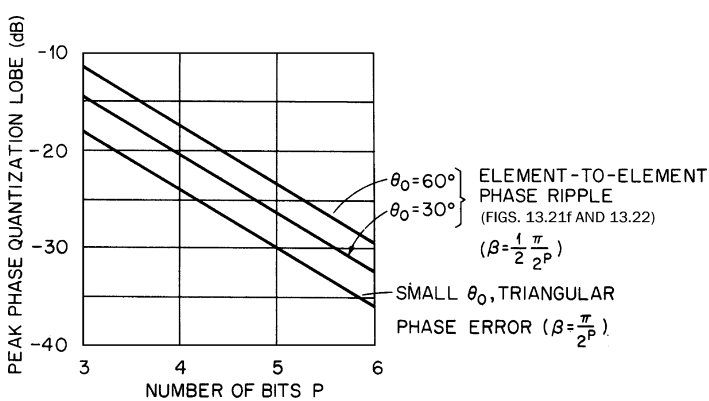

FIGURE 13.23 Peak sidelobes due to phase quantization

The variable phase shifter is then programmed to account for this additional insertion phase. With a spherical or quadratic law of insertion phase variation, as obtained with optical-feed systems (Section 13.8), the reductions in peak quantization lobes are equivalent to adding 1 bit to the phase shifters in a 100-element array, 2 bits in a 1000-element array, and 3 bits in a 5000-element array.

Amplitude Quantization. When the aperture of a phased array is divided into equal subarrays, then the amplitude distribution across each subarray is constant. Aperture taper for the antenna is approximated by changing the amplitude from subarray to subarray, and quantization lobes arise from these discontinuities. The value of these lobes may be estimated from the various results shown in Figure 13.21 or actually computed by summing all contributions at the known quantization (grating) lobe angles. The distribution becomes smoother as the number of subarrays is increased or as they are interlaced.

13.7 BANDWIDTH OF PHASED ARRAYS

The phenomenon of focusing an array is the result of the energy from each element adding in-phase at some desired point within the antenna. When energy is incident normal to the array, each element receives the same phase independent of frequency. When energy is incident from some angle other than normal, the phase difference from the planar phase front to each element is a function of frequency and most phased arrays with phase shifters become frequency-dependent. This same phenomenon can be viewed in the time domain. As shown in Figure 13.24, when a pulse of energy is incident at an angle other than normal, the energy is received earlier at one edge of the array than at the other edge and a period of time must elapse before energy appears in all elements. The concept of aperture fill time, $T = L/c \sin \theta_0$, is just another way of explaining the bandwidth of a phased array.

The bandwidth of phased arrays is described by Frank[79] as being composed of two effects: the aperture effect and the feed effect. In both effects, it is the path-length differences that contribute to the bandwidth sensitivity of a phased array. For a parallel-fed

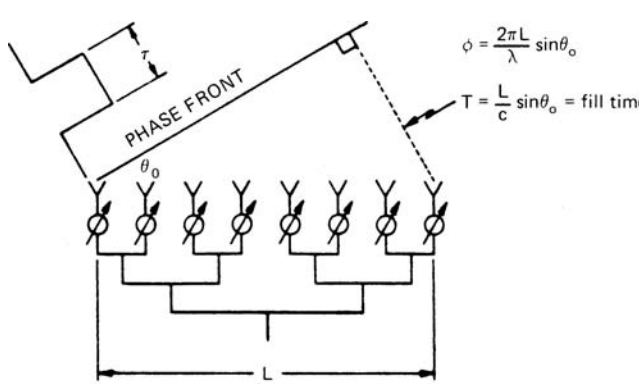

FIGURE 13.24 Aperture-fill-time parallel-fed array (*after J. Frank*[79] © *Artech House 1972*)

array (equal line length), the feed network does not contribute to a change in phase with frequency, and so only the aperture effect remains. This will be discussed first, and the effect of the feed will follow.

Aperture Effects. When energy is incident on an array at an angle other than broadside (Figure 13.24), the phase required on the edge element is $\psi = (2\pi L)/\lambda \sin \theta_0$. Note the λ in the denominator. This indicates that the required phase is frequency-dependent. If frequency is changed and the phase shifters are not changed, the beam will move. For an equal-line-length feed, the beam shape will be undistorted (in sine space) and the beam will move toward broadside as the frequency is increased. If the phase shifters are replaced by time-delay networks, then the phase through the time-delay networks will change with frequency and the beam will remain stationary.

When phase shift (independent of frequency) is used to steer the beam, the beam is steered to a direction θ_0 with a phase of

$$\psi = \frac{2\pi x}{\lambda_1} \sin \theta_0 = \frac{2\pi x}{c} f_1 \sin \theta_0$$

on the element located a distance x from the array center. At frequency f_2 this same phase setting steers the beam to a new direction, $\theta_0 + \Delta\theta_0$, which is shown in Frank[79] to be

$$\Delta\theta_0 = \frac{\Delta f}{f} \tan \theta_0 \qquad \text{(rad)} \tag{13.26}$$

As the frequency is increased, the beam scans toward broadside by an angle that is independent of the aperture size or beamwidth. However, the permissible amount that the beam may scan with frequency is related to the beamwidth because pattern and gain deteriorations are a function of the fractional beamwidth scanned. The angle that the beam actually scans, on the other hand, is related to the percentage bandwidth. A bandwidth factor may, therefore, be defined in terms of the broadside beamwidth:

$$\text{Bandwidth factor} = K = \frac{\text{bandwidth}\,(\%)}{\text{beamwidth}\,(^\circ)}$$

A reasonable criterion is to limit the bandwidth so that the beam never scans by more than ± one-fourth of a local beamwidth frequency, i.e.,

$$\text{Criterion:} \left| \frac{\Delta\theta_0}{\theta_B\ (\text{scanned})} \right| \le \frac{1}{4}$$

With a scan of 60°, this gives $K = 1$, and in terms of broadside beamwidth the limit is

$$\text{Bandwidth}\ (\%) = \text{beamwidth}\ (^\circ) \quad \text{(CW)}$$

For example, if the array has a beamwidth of 2° this criterion permits a 2% change in frequency prior to resetting the phase shifters. This allows the beam to move from one-fourth beamwidth on one side of the desired direction to one-fourth beamwidth on the other side as the frequency changes by 2%. At smaller scan angles, the effect is reduced as given by Eq. 13.26, and broader-band operation is possible.

The explanation given above applies to an antenna operating at a single (CW) frequency and describes how the beam moves as this frequency is changed.

However, most radars are pulsed and radiate over a band of frequencies. For a beam scanned from broadside, each spectral component is steered to a slightly different direction. To determine the composite effect of the components, it is necessary to add the far-field patterns of all spectral components. This analysis has been performed[80,81] and it is apparent that the overall antenna gain of the pulse will be less than that of a single spectral component that has maximum gain in the desired direction. As with the CW situation, the greatest loss occurs at the maximum scan angle, which is assumed to be 60°. For this situation, the criterion chosen is to allow a spectrum that loses 0.8 dB of energy on target due to frequency-scanned spectral components. For a beam scanned to 60°, this becomes

$$\text{Bandwidth (\%)} = 2 \text{ beamwidth (°)} \quad \text{(pulse)}$$

Note that this is twice the bandwidth permitted for the CW situation. Another way of analyzing this phenomenon is in terms of aperture fill time. As shown in Figure 13.24, the time it takes to fill the aperture with energy is

$$\tau = \frac{L}{c} \sin \theta_0$$

If the bandwidth is chosen to be equal to the aperture fill time $\tau = L/c \sin \theta_0$, this is equivalent to bandwidth (%) = 2 beamwidth (°). Hence, a loss of 0.8 dB can be expected if the pulse width is equal to the aperture fill time. Longer pulses will have less loss. The exact amount of the loss will depend on the specific spectrum transmitted, but the variation will amount to less than 0.2 dB for most waveforms. Rothenberg and Schwartzman[82] provide details and also treat the problem as a matched filter.

The preceding discussion assumes an equal-path-length feed. However, it is unlikely that a feed will provide exactly equal path lengths. It will suffice to have the path lengths kept within one wavelength of each another. The phase errors introduced can then be corrected by programming the phase shifters. This will have the beneficial effect of breaking up the quantization errors and thereby reducing quantization lobes.

Feed Effect. When an equal-path-length feed is not in use, the feed network will produce a change in phase with frequency. In some cases, such as Rotman lens[83] or equal-length Blass matrix[84], the feed can actually compensate for the aperture effect and produce a beam direction that is independent of frequency. However, the more conventional feeds tend to reduce the bandwidth of the array.

End-Fed Series Feed. An end-fed series array is shown in Figure 13.31*a* later in this chapter. The radiating elements are in series and progressively farther and farther removed from the feed point. When the frequency is changed, the phase at the radiating elements changes proportionately to the length of feed line so that the phase at the aperture tilts in a linear manner and the beam is scanned. This effect is useful for frequency-scanning techniques, but in the case of phased arrays, it is undesirable and reduces the bandwidth. It has been shown previously that with phased arrays, the pointing direction of a scanned beam also changes with frequency (Eq. 13.26) because phase rather than time delay is adjusted. These two changes in beam-pointing direction may add or subtract, depending on the direction in which the beam has been scanned. The worst case will be considered here.

With a change in frequency, a nondispersive transmission line having free-space propagation characteristics and a length L equal to the size of the aperture that it feeds will produce a linear-phase variation across the aperture with a maximum value at the edges of

$$\Delta\psi_{\max} = \frac{\Delta f}{f}\frac{2\pi L}{\lambda} \qquad \text{rad}$$

where $\Delta f/f$ is the fractional change in frequency. This linear-phase progression across the aperture will scan the beam by

$$\Delta\theta_0 = \frac{\Delta f}{f}\frac{1}{\cos\theta_0} \qquad \text{rad}$$

For one direction of scanning, this effect will add to the aperture effect; for the opposite direction, it will tend to cancel the aperture effect. In a waveguide, with the guide wavelength denoted λ_g, the effect is more pronounced and the resultant change in beam position is

$$\Delta\theta_0 = \frac{\lambda_g}{\lambda}\frac{\Delta f}{f}\frac{1}{\cos\theta_0} \qquad \text{rad}$$

When analyzing an end-fed series feed, it is necessary to consider both the feed effect and the aperture effect. The total frequency scan of this feed will be

$$\Delta\theta_0 = \frac{\Delta f}{f}\tan\theta_0 \pm \frac{\lambda_g}{\lambda}\frac{\Delta f}{f}\frac{1}{\cos\theta_0} \qquad \text{rad} \qquad \text{(CW)}$$

Center-Fed Series Feed.[85] A center-fed array (Figure 13.25) can be considered as two end feeds. Each feed controls an aperture that is half the total and, therefore, has twice the beamwidth. As the frequency is changed, each half of the aperture scans in the opposite direction. This initially creates a broader beam with reduced gain. As frequency continues to change, the two beams will eventually split apart. At broadside, the center-fed antenna has poorer performance than a parallel feed since each half scans. However, at 60° scan the compensation on one-half of the array assists in keeping the gain comparable to that of a parallel feed. From the viewpoint of gain reduction, the criterion for a center-fed array is

$$\text{Bandwidth}\,(\%) = \frac{\lambda}{\lambda_g}\,\text{beamwidth}\,(^\circ) \quad \text{(CW)}$$

where λ_g is the waveguide wavelength.

However, from the viewpoint of sidelobes, this criterion may be unacceptable. For a low-sidelobe design, either CW or pulsed, the sidelobes for this feed should be calculated because a change in frequency no longer produces a translated beam but rather a broader beam composed of two translated beams.

Space Feed. The space (optical) feed can be considered to be somewhat between a parallel feed and a center-fed series feed. With a very long focal length, the space feed approximates a parallel feed. With a very short focal length it approximates a

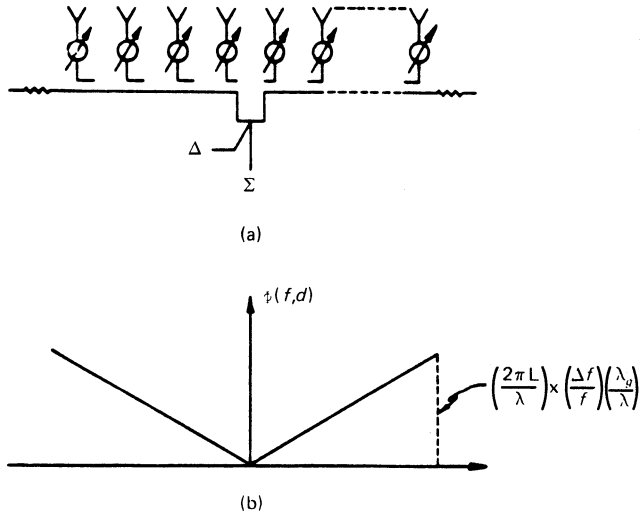

FIGURE 13.25 Center-fed series array (*after J. Frank*[79] © *Artech House 1972*): (*a*) center-fed series feed and (*b*) gabled phase due to feed

center-fed series feed. Because the bandwidth performance of each is comparable, the optical-feed criterion is

$$\text{Bandwidth (\%)} = \text{bandwidth (°)} \quad \text{(CW)}$$

Table 13.2 summarizes the bandwidth criteria for the various feed networks. Both the CW criterion and the comparable pulse criterion are given.

Broad Instantaneous Bandwidth. For a stationary beam in space, independent of frequency, it is necessary to use time delay rather than phase steering. It is not practical to provide a time-delay network at each element in a phased array because

TABLE 13.2 Bandwidth Criteria for Several Feed Networks*

Feed	CW Bandwidth (%)	Pulse Bandwidth (%)
Equal line length	Beamwidth	2 × beamwidth
End-fed series	$\frac{1}{\left(1+\frac{\lambda_g}{\lambda}\right)}\times$ beamwidth	$\frac{2}{\left(1+\frac{\lambda_g}{\lambda}\right)}\times$ beamwidth
Center-fed series	$\frac{\lambda}{\lambda_g}\times$ beamwidth	$2\,\frac{\lambda}{\lambda_g}\times$ beamwidth
Space-fed (optical)	Beamwidth	2 × beamwidth

* *After Frank*[79]
NOTE: All beamwidths are in degrees and refer to the broadside beamwidth: λ_g = guide wavelength and λ = free-space wavelength.

these networks are expensive and lossy and contain errors. An alternative is to use a broadband beam-switching technique such as the equal-line-length Blass matrix[84] or a Rotman lens.[83] For 2D scanning these techniques become quite complex.

Another technique for improving the bandwidth by a considerable factor is to use an array of subarrays. The radiating elements of a phased array may be grouped into subarrays where time-delay elements are added. This is shown in Figure 13.26. The antenna may be regarded as an array of subarrays. The subarray pattern forms the element factor; it is steered by phase shifters in the desired direction, but it scans with frequency as indicated by Eq. 13.26. The array factor is scanned by adjusting the frequency-independent time-delay elements. All subarrays are steered in the same manner. The total radiation pattern is the product of the array factor and the element factor. A change in frequency gives rise to grating lobes rather than shifts of the beam position. This can be seen from Figure 13.27. The subarray pattern is shown at the design frequency f_0 and is seen to have a null at the position of the grating lobe. As frequency is changed by δf, the pattern is scanned. It is shown dashed in a position where it has been scanned by a little more than half of its beamwidth. This is clearly too much, for the product of array and element factors gives two beams of equal amplitude.

The loss in gain and the magnitude of the grating lobe are functions of the fractional subarray beamwidth that has been scanned as a result of the change in frequency. The results may be expressed in terms of the bandwidth factor K (referred to as the *subarray broadside beamwidth*).

Figure 13.28 shows these values as functions of K for a scan of 60°.

The value previously used for scanning 60° was $K = 1$ and this value appears acceptable here, where the relevant beamwidth is the broadside beamwidth of the subarray. Thus, if the aperture is split into N subarrays in one plane, with time-delay networks at each subarray level, the bandwidth is increased by a factor of N. This same bandwidth criterion leads to a reduction in gain of about 0.7 dB and a grating lobe of about −11 dB at the edges of the band with 60° of scan. Interlacing of subarrays can reduce the grating lobes.

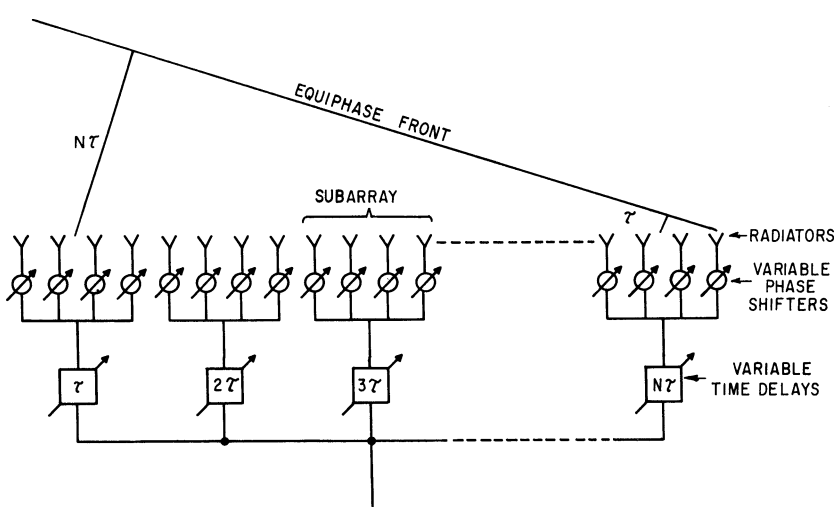

FIGURE 13.26 Phased array using subarrays with time delay

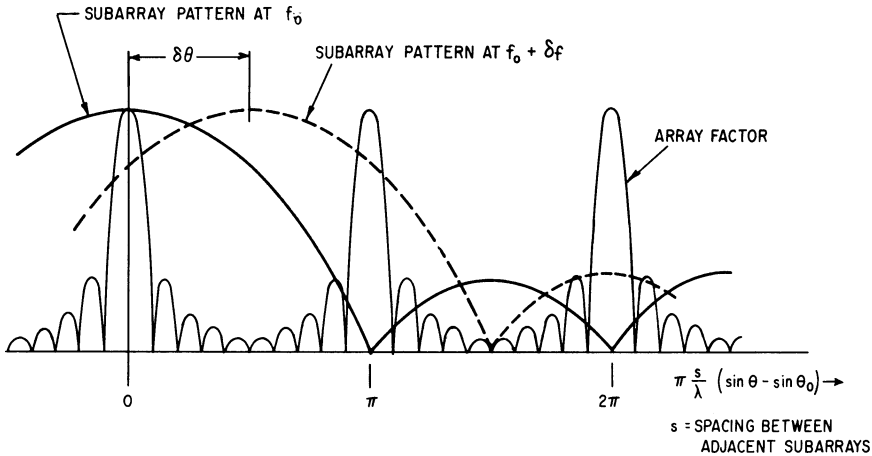

FIGURE 13.27 Generation of grating lobes by a change of frequency

The monopulse null position is unaffected by the behavior of the subarrays as long as they all respond in the same way. The null position is determined only by the time-delay networks behind the subarray and corresponds to the array-factor null, which is unaffected when multiplied by the subarray pattern.

Time-Delay Networks. Figure 13.29*a* shows a time-delay network that is digitally controlled by switches. The total delay path length that has to be provided non-dispersively amounts to $L \sin \theta_{max}$, where θ_{max} is the maximum scan angle for the aperture L. The smallest bit size is about $\lambda/2$ or λ, with the precise setting adjusted by

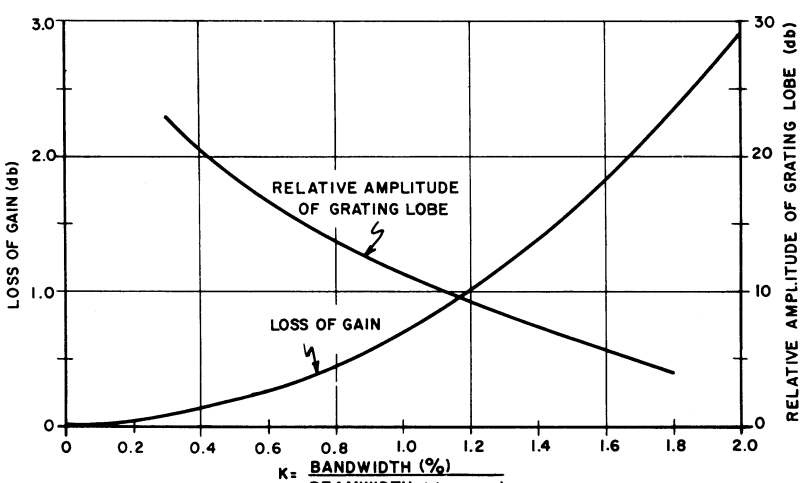

FIGURE 13.28 Loss of gain and grating-lobe amplitude as functions of bandwidth (phased subarrays with time delay, scanned 60°). The value of the grating lobe will be modified by the element pattern.

an additional variable phase shifter. A 1° beam scanned 60°, for example, requires a time delay of 6 bits, the largest being 32 wavelengths, as well as an additional phase shifter. The tolerances are tight, amounting in this case to a few degrees out of about 20,000 and are difficult to meet. Problems may be due to leakage past the switch, to a difference in insertion loss between the alternate paths, to small mismatches at the various junctions, to variations in temperature, or to the dispersive characteristics of some of the components. Painstaking design is necessary. The switches may be diodes or circulators. Leakage past the switches may be reduced by adding another switch in series in each line. The difference in insertion loss between the two paths may be equalized by padding the shorter arm. The various problems have been comprehensively assessed and analyzed by Lincoln Laboratory.[45]

On transmitting, the tolerances are less severe because the requirements are usually for power on target rather than for accurate angle determination or low sidelobes.

Figure 13.29*b* shows another configuration that has the advantage of simplicity. Each of the switchable circulators connects either directly across (counterclockwise) or via the short-circuited length. Isolation in excess of 30 dB is required. It is clear that the insertion loss of time-delay circuits is very high for most practical systems. They would, therefore, precede a final power amplifier for transmitting and follow a preamplifier for receiving.

A further method of providing delay is possible by translating the problem from the microwave domain and delaying at IF.

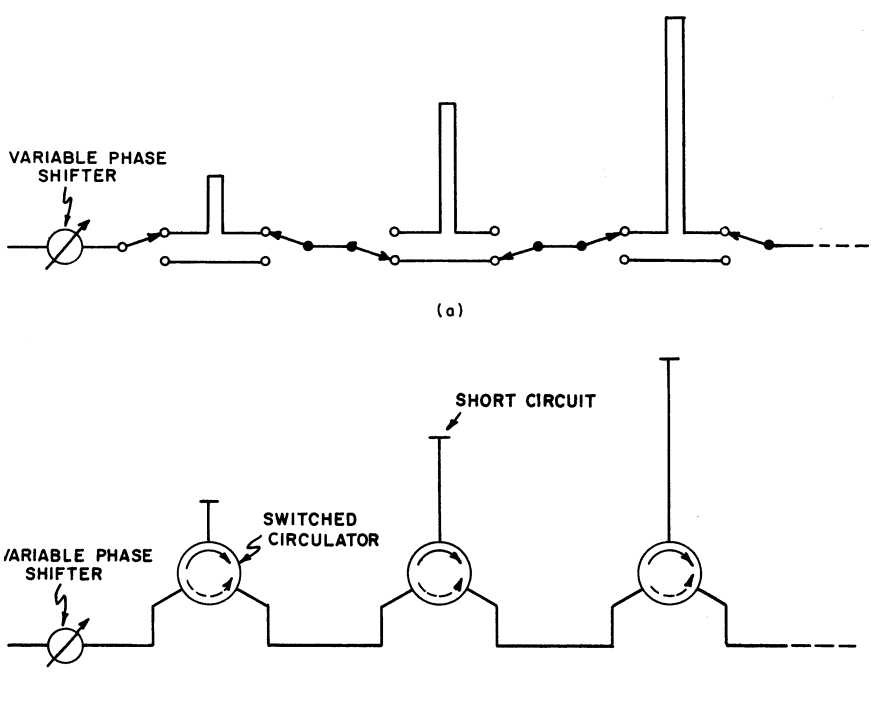

FIGURE 13.29 Time-delay configurations: (*a*) time delay by choosing upper or lower paths and (*b*) time delay by using switched circulators

13.8 FEED NETWORKS (BEAMFORMERS)

Optical-Feed Systems. Phased arrays may be in the form of lens arrays or reflectarrays, as shown in Figure 13.30, where an optical-feed system provides the proper aperture illumination. The lens has input and output radiators coupled by phase shifters. Both surfaces of the lens require matching. The primary feed should be designed with care and can be complex to give the desired aperture amplitude distribution with low spillover losses. The transmitter feed can be separated from the receiver feed by an angle α, as shown in Figure 13.30. The phase shifters are then reset between transmitting and receiving so that in both cases the beam points in the same direction. This method allows flexibility in optimizing the transmitter aperture distribution, perhaps for maximum power on the target, and separately optimizing the receiver sum and difference patterns for low sidelobes. Since a change in feed position corresponds to scanning with time delay, additional feeds may be added to provide several time-delay-compensated directions of scan for a corresponding increase in bandwidth.

The phasing of the antenna has to include a correction for the spherical phase front. This can be seen (Figure 13.30*a*) to amount to

$$\frac{2\pi}{\lambda}\left(\sqrt{f^2+r^2}-f\right)=\frac{\pi}{\lambda}\frac{r^2}{f}\left[1-\frac{1}{4}\left(\frac{r}{f}\right)^2+\ \ldots\right]$$

With a sufficiently large focal length, the spherical phase front may be approximated by that of two crossed cylinders, permitting the correction to be applied simply with row-and-column steering commands.

Correction of a spherical phase front with the phase shifters reduces peak phase-quantization lobes (Section 13.6). Space problems may be encountered in assembling an actual system, especially at higher frequencies, because all control circuits have to be brought out at the side of the aperture of the lens array.

Multiple beams may be generated by adding further primary feeds. All the beams will be scanned simultaneously by equal amounts in sin θ.

The reflectarray shown in Figure 13.30*b* has general characteristics similar to those of the lens. However, the same radiating element collects and radiates after reflection. Ample space for phase-shifter control circuits exists behind the reflector. To avoid aperture blocking, the primary feed may be offset as shown. As before, transmitting and receiving feeds may be separated. Multiple beams are again possible with additional feeds.

The phase shifter must be reciprocal so that there is a net controllable phase shift after passing through the device in both directions. This rules out frequently used nonreciprocal ferrite or garnet phase shifters.

Constrained Feeds. The optical-feed system divides power very simply in one step from the feed to the many elements on the aperture. In contrast, the constrained-feed system uses many steps. For a high-performance low-sidelobe system, each of these power-dividing steps has to be well matched over the band. If mismatches are present, they will be separated by many wavelengths and will add up to give frequency-sensitive phase and amplitude perturbations at the aperture. In general, these perturbations will be different for the monopulse sum and difference patterns, so that only a common average can be compensated by calibration.

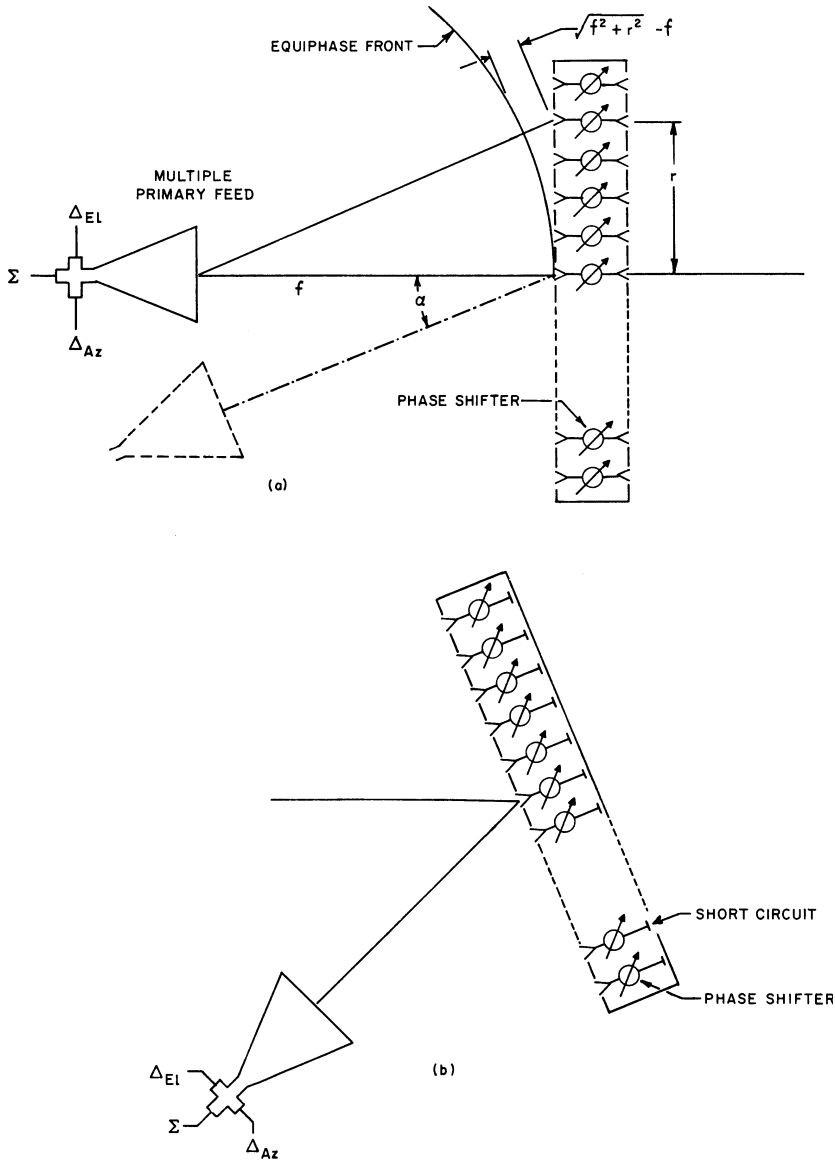

FIGURE 13.30 Optical-feed systems: (*a*) lens array and (*b*) reflectarray

Series Feeds. Figure 13.31 shows several types of series feeds. In all cases except *d*, the electrical path length to each radiating element has to be computed as a function of frequency and taken into account when setting the phase shifters. Type *a* is an end-fed array. It is frequency-sensitive and leads to more severe bandwidth restrictions than most other feeds. Type *b* is center-fed and has almost the same bandwidths as a

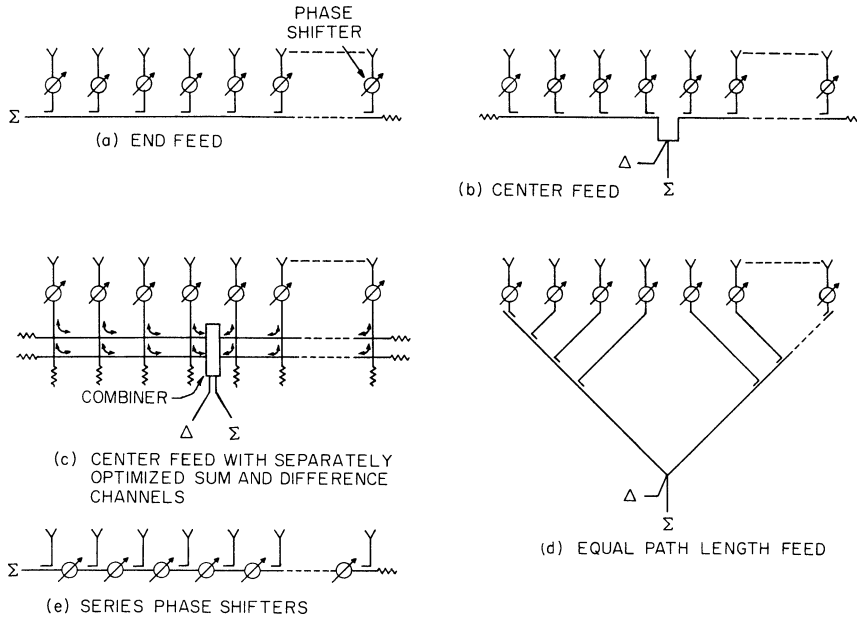

FIGURE 13.31 Series-feed networks

parallel-feed network. Sum- and difference-pattern outputs are available, but they have contradictory requirements for optimum amplitude distributions that cannot both be satisfied. As a result, either good sum or good difference patterns can be obtained. At the cost of some additional complexity, the difficultly can be overcome by the method shown in Figure 13.31*c*. Two separate center-fed feed lines are used and combined in a network to give sum- and difference-pattern outputs.[86] Independent control of the two amplitude distributions is possible. For efficient operation, the two feed lines require distributions that are *orthogonal*, that is, that give rise to patterns where the peak value of one coincides with a null from the other and aperture distributions are respectively even and odd.

A very wideband series feed with equal path lengths is shown in Figure 13.31*d*. If the bandwidth is already restricted by phase scanning, then very little advantage is obtained at the cost of a considerable increase in size and weight. The network in Figure 13.31*e* gives simplicity in programming because each phase shifter requires the same setting. The insertion loss increases for successive radiators, and the tolerances required for setting the phases are high. This type is not commonly used.

Parallel Feeds. Figure 13.32 shows a number of parallel-feed systems. They frequently combine a number of radiators into subarrays, and the subarrays are then combined in series or in parallel to form sum and difference patterns.

Figure 13.32*a* shows a *matched corporate feed*, which is assembled from matched hybrids. The out-of-phase components of mismatch reflections from the aperture and of other unbalanced reflections are absorbed in the terminations. The in-phase and

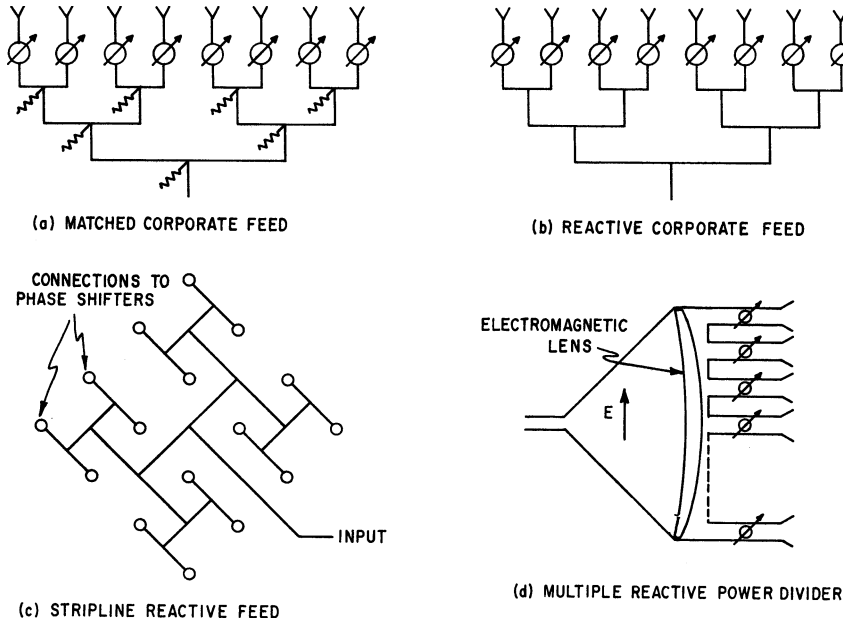

FIGURE 13.32 Parallel-feed networks

balanced components are returned to the input. To break up periodicity and reduce peak quantization lobes (Section 13.6), small additional fixed phase shifts may be introduced in the individual lines and compensated by corresponding readjustments of the phase shifters.

The reactive feed network shown in Figure 13.32*b* is simpler than the matched configuration. It has the disadvantage of not terminating unbalanced reflections that are likely to be at least partly reradiated and thus contribute to the sidelobes. A stripline power divider is shown in Figure 13.32*c*, and a constrained optical power divider using an electromagnetic lens is shown in Figure 13.32*d*. The lens may be omitted and the correction applied at the phase shifters. With nonreciprocal phase shifters, a fraction of the power reflected from the aperture will then be reradiated (as sidelobes) rather than returned to the input. The amplitude distribution across the horn is given by the waveguide mode. It is constant with an E-plane horn as shown.

Subarrays. The phased-array aperture may be divided into subarrays, all similar to simplify manufacturing and assembly. Beamforming now requires combining the subarrays for suitable sum and difference patterns. Figure 13.33*a* shows a method of combining opposite subarrays into their sums and differences. All sum channels are then added with proper weighting to obtain the desired amplitude distribution. The difference channels are treated similarly with independent amplitude weighting. This method may be extended to include combinations in the other plane.

Amplification on receiving or on both receiving and transmitting may be convenient at the subarray level. On receiving, the noise figure is established by the

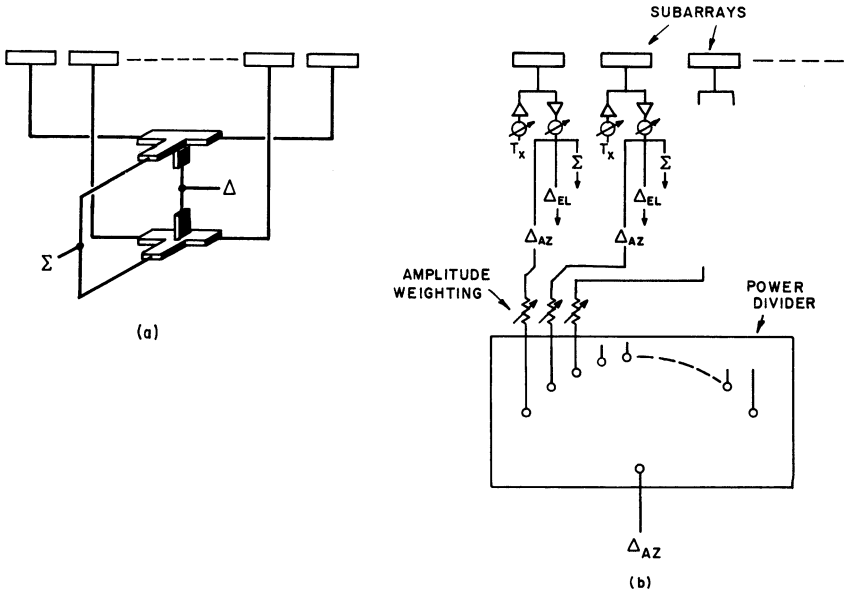

FIGURE 13.33 Combination of subarrays to form sum and difference channels: (*a*) combining opposite subarrays and (*b*) combining subarrays after amplification

preamplifier so that further processing may include lossy circuits. The receiving channel may be split three ways, as indicated in Figure 13.33*b*, into the sum and the elevation and azimuth difference channels. These are then weighted and summed with corresponding outputs from the other subarrays. On transmitting, all separate power amplifiers may be energized equally to give maximum power on the target. The addition of phase shifters shown at the subarray level simplifies the beam-steering computation, permitting all subarrays to receive identical steering commands. They may be replaced by time-delay circuits giving a wide instantaneous bandwidth (Section 13.7).

The simple method of providing TR (transmit-receive) switching can be obtained by combining two halves of a subarray with a four-port hybrid junction. The transmitter input into one port energizes both halves of the aperture, for example, in phase. The receiver, connected to the remaining port, then requires that the phase shifters of half the aperture give an additional phase shift of π during the receiving period. This is easily programmed.

Multiple receive beams may be formed by combining the subarrays after amplification in as many different ways as separate beams are required. The limitation is that the beams have to lie within the beamwidth of the subarray in order to avoid excessive grating lobes. A cluster of such simultaneous receiver beams requires a wider transmitter beam. This may be obtained efficiently from the same antenna with a gabled or spherical phase distribution.

With identical subarrays, a desired aperture amplitude taper (for low sidelobes) is applied with a granularity that depends on their size and shape. The resulting amplitude steps will cause quantization lobes (Section 13.6).

13.9 PHASE SHIFTERS

The three basic techniques for electronic beam steering are (1) frequency scanning, (2) beam switching, and (3) phase scanning with phase shifters. Of the three techniques, the use of phase shifters is by far the most popular, and considerable effort has gone into the development of a variety of phase shifters. Phase shifters can be separated into two categories: reciprocal and nonreciprocal. The reciprocal phase shifter is not directionally sensitive. That is, the phase shift in one direction (e.g., transmit) is the same as the phase shift in the opposite direction (e.g., receive). Therefore, if reciprocal phase shifters are used, it is not necessary to switch phase states between transmit and receive. With a nonreciprocal phase shifter, it is necessary to switch the phase shifter (i.e., change phase state) between transmit and receive. Typically, it takes a few microseconds to switch nonreciprocal ferrite phase shifters. During this time, the radar is unable to detect targets. For low pulse repetition frequency (PRF) radars [e.g., 200 to 500 pulses per second (pps)], this may not cause a problem. For example, if the PRF is 200 pps (or Hz), the time between pulses is 500 μs. If the switching time for the phase shifter is 10 μs, only 2% of the time is wasted and less than 1.0 nmi of minimum range is lost. On the other hand, if the PRF = 50 kHz, the time between pulses is 20 μs, and it would not be possible to tolerate 10 μs of dead time for the switching of phase shifters.

All diode phase shifters are reciprocal along with certain types of ferrite phase shifters. It is worth noting that, owing to losses associated with their magnetic properties, ferrite phase shifters are almost never used at frequencies below 3 GHz. Diode phase shifters, in contrast, improve as the frequency gets lower.

There are three basic types of phase shifters that typically compete for use in a phased array. They are (1) the diode phase shifter, (2) the nonreciprocal ferrite phase shifter, and (3) the reciprocal (dual-mode) ferrite phase shifter. Each has its strengths, and the choice of which to use is highly dependent on the radar requirements. Each will be discussed in turn. For solid-state systems, diodes are used and can be switched in a fraction of a microsecond.

Diode Phase Shifters.[87–90] Diode phase shifters are typically designed by using one of three techniques: (1) switched-line, (2) hybrid-coupled, and (3) loaded-line. These are shown diagrammatically in Figure 13.34. The switched-line technique simply switches in lengths of line in binary increments (e.g., 180°, 90°, and 45°) and requires a set of diodes for each bit. The diodes are used as switches to control which bits are activated to achieve a particular phase state.

The hybrid-coupled technique uses a microwave hybrid and effectively changes the distance at which the reflection takes place. This technique is usually used in binary increments, and an additional set of diodes is required for each phase state.

The diode phase shifters described above are limited in their ability to handle high peak power. Depending on their size and frequency, they are normally restricted to power levels of less than 1 kW. For higher power levels, the loaded-line technique is used. The diodes are used to switch in increments of capacitance and inductance that provide small changes in phase. Because the diodes are decoupled from the main transmission line, they need to handle only modest amounts of power in each diode. Very high power (i.e., kilowatt) configurations are possible. The technique does require many diodes, and the phase shifters are typically large and bulky as compared with the switched-line and hybrid-coupled techniques.

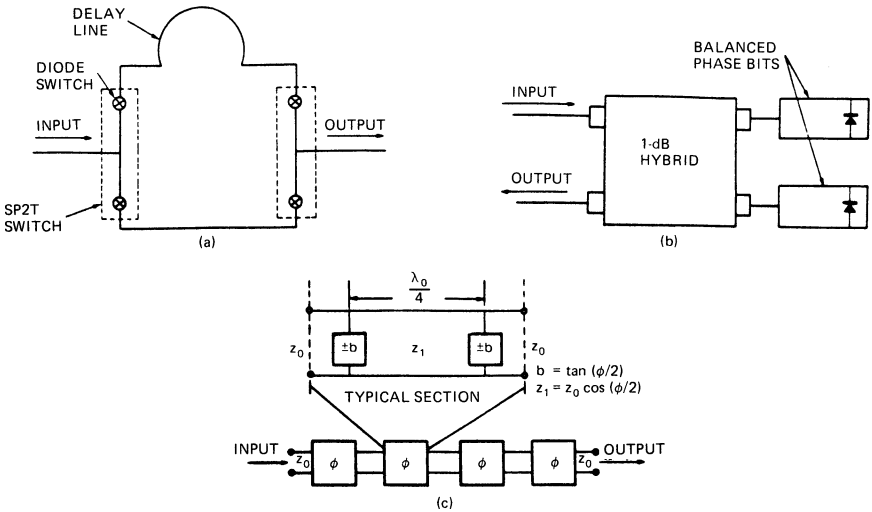

FIGURE 13.34 Diode phase-shifter configurations (*after L. Stark et al.*[87]): (*a*) switched-line phase bit, (*b*) hybrid-coupled phase bit, and (*c*) loaded-line phase bit

Diode phase shifters have the advantage of being small and light in weight (except for high-power devices). They are suitable for stripline, microstrip, and monolithic configurations. The main disadvantage of the diode phase shifter is that an additional set of diodes is normally required for each additional bit. As lower-sidelobe antennas are required, the number of bits increases. For low sidelobe antennas, 5, 6, or 7 bits may be required. As the number of bits increases, both cost and loss of the diode phase shifters are also increased. For active arrays, the phase shifter losses are not of significance because they occur prior to the power amplifier on transmit and after the low-noise amplifier on receive. This is not the case with most ferrite devices.

Ferrite Phase Shifters. Most ferrite phase shifters are nonreciprocal,[91–93] and their early versions used discrete lengths of ferrite (as shown in Figure 13.35) to implement each of the bits (180°, 90°, 45°, etc.). In this configuration, a current pulse is passed through each bit, and the ferrite toroid is saturated. When the current is removed, the ferrite toroid is said to be *latched* and retains its magnetization owing to its hysteresis properties. If the current is in a forward direction, the ferrite is latched with a particular phase (e.g., 180°). The ferrite maintains the phase until a current pulse in the opposite direction is applied. The ferrite phase shifter is then latched to the reference phase (0°). This change in phase with a change in current direction is due to the nonreciprocal nature of the device. As mentioned, early devices saturated each bit so that a ferrite toroid and electronic driver were required

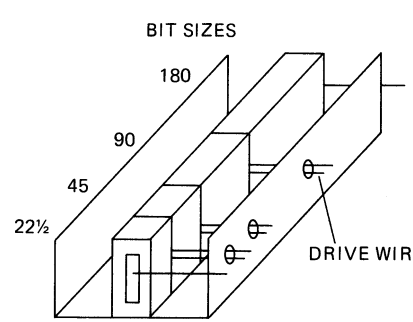

FIGURE 13.35 Digital ferrite phase shifter using toroids (*after L. Stark*[87])

to control each bit individually. Other phase shifters use a single toroid and a single driver.[94,95] In this configuration, the phase shifter is latched on a minor hysteresis loop by only partially magnetizing the ferrite. The distinct advantage of this technique is that any number of bits may be implemented while using only a single toroid. They have the advantage of low loss and relatively high power operation. Devices that handle up to 100 kW of peak power have been built. They are amenable to waveguide construction and are heavier and bulkier than comparable diode devices.

In summary, diodes and nonreciprocal ferrite phase shifters are viable competitors. At L band and lower, diode phase shifters are an obvious choice. At S band and higher, ferrites should continue to hold an edge in higher-power systems and where additional bits are needed for the low phase errors required for low-sidelobe antennas. These comments do not apply for the solid-state systems described below. Ferrite phase shifters are more temperature-sensitive than diodes, and the phase will change with a change in temperature. This can be controlled by keeping the temperature constant (within a few degrees) across the array. A more common technique is to sense the temperature at several locations in the array and then correct the phase commands to the phase shifters.

13.10 SOLID-STATE MODULES[96–98]

A solid-state module may be connected to every radiating element or to every subarray of a phased array antenna, forming what is sometimes called an *active aperture*. Applications range from ultrahigh frequency (UHF) for surveillance to X band and above for airborne systems.

A typical module is shown in simple schematic in Figure 13.36. It consists of a transmitter amplifier chain, a preamplifier for receiving, a shared phase shifter with driver, and circulators and/or switches to separate the transmit and receive paths (the gain around the loop must be less than unity to avoid oscillations).

Power amplifiers for transmitting at the element level would typically have a gain of 30 dB or more to compensate for the loss of power dividing in the beamformer. Transistors are capable of generating high average power but only relatively low peak power. High duty-cycle waveforms (10 to 20%) are therefore required to transmit enough energy efficiently. This lack in high peak power is the main disadvantage of the solid-state modules in phased array radars. To a great extent, it can be compensated for by using more pulse compression in the receiver and extra-wide bandwidth to counteract jamming, but at the cost of increased signal processing. An important advantage of transistors is their potential for wide bandwidth.

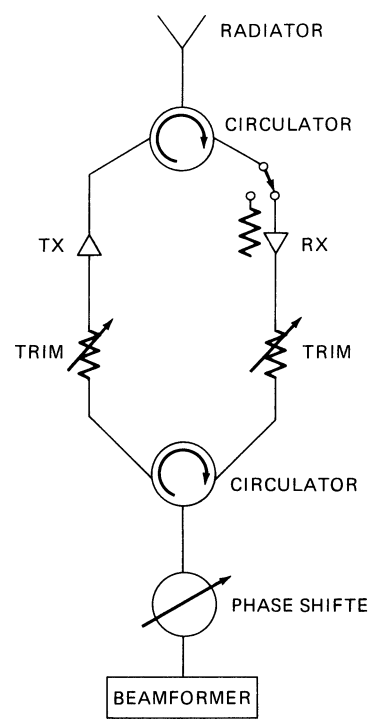

FIGURE 13.36 Typical solid-state module

The receiver requires an early gain of typically 10 to 20 dB to adequately establish a low noise figure and allow for phase shifting and beamforming losses. The module also receives interfering signals from all directions within the element pattern (not simply the antenna pattern), at all frequencies in the band. Tight tolerances between modules are needed to provide amplitude and phase tracking over the band for low-sidelobe performance. An electronically programmable gain adjustment may be helpful to correct module-to-module variations, allowing less demanding specifications. The trimmer would also provide a degree of freedom in aperture control for special situations. Because the noise figure has been established, the feed network may be split to give separate optimum aperture amplitude distributions for transmitting as well as for receiving on sum and difference channels. In an alternative configuration, the feed network could be designed for a constant amplitude aperture distribution to give highest transmit power on the target, and the receiver gain control could be used to provide an amplitude taper for the sum channel. Perhaps a secondary feed system could be added for the difference channels. Poirier[97] has analyzed this case, the effect on noise, and the degradation due to amplitude quantization steps.

The module phase shifter operates at low-signal power levels. Its insertion loss may be high because it is followed by amplification on transmit and preceded by amplification on receive. Diode phase shifters are, therefore, quite permissible even with many bits (e.g., 5, 6, or 7 bits for low sidelobes). Variations in insertion loss may be compensated for dynamically with the gain adjustment.

The circulator at the high-power side provides an impedance match to the power amplifier and may be adequate by itself for protecting the receiver. In Figure 13.36, the module is shown augmented by a switch that causes absorption of power reflected from antenna mismatches and also gives added protection to the receiver during transmission. If weight is an important consideration, as it would be in a space-based system, then the circulator could be replaced by diode switches requiring additional logic and driving circuitry.

13.11 MULTIPLE SIMULTANEOUS RECEIVE BEAMS

With the proliferation of ballistic missiles, future shipboard radar systems will probably need multi-mission capability, which includes both anti–air warfare (AAW) and ballistic missile defense (BMD). The BMD requirement to discriminate small radar cross section (RCS) re-entry vehicles (RVs) at long ranges requires that active array radars have a large power-aperture-gain/loss-noise temperature (PAG/LT), which is a measure of the sensitivity of the radar. Increasing the output power of a T/R module only increases the transmit power component of the PAG product. However, adding an additional T/R module to the array increases each of the components of the PAG: the transmit power, the receive aperture, and the transmit gain. Therefore, radars with a BMD function typically have a large number of elements, which results in a large aperture. Because a large antenna aperture produces a narrow antenna beamwidth, the volume search function will require scanning a large number of beam positions.

Naval ships need to operate in littoral (close to land) environments, as well as in the open ocean. The desire to operate closer to land requires shipboard radars to have the capability to reject high clutter returns. High clutter rejection is usually achieved through the use of pulse doppler waveforms in the first few elevation beam positions.

In addition, many of the radar waveforms may be designed to propagate out to the instrumented range of the radar. As a result, a major component of the dwell time at each beam position is the time required for the pulse to propagate to the instrumented range and back. This long propagation time, combined with the large number of beam positions due to a narrow antenna beamwidth and a pulse doppler waveform with a large number of pulses, results in unsatisfactory long search frame times when using a single beam radar.

If the active array radar is sized for long-range detection of ballistic missiles, the radar will most likely have sufficient power to detect other targets. A cluster of multiple simultaneous receive beams can be used to trade energy for a reduction in the volume search frame time. The use of multiple simultaneous receive beams will reduce the search frame time, since many beam positions are searched at the same time. When using multiple simultaneous receive beams, the transmit beam can be broadened by beam spoiling so that the 3-dB beamwidth is larger than that of a uniformly illuminated array with a linear phase front. Broadening the beam on transmit reduces the gain of the transmit beam, but this loss in gain may be necessary to produce the search frame time required. On receive, multiple beams are simultaneously formed in a cluster that covers the volume illuminated by the transmit beam. Each receive beam has the full gain and beamwidth of a single beam array with the same aperture dimensions. In the cluster of receive beams, each of the receive beams may be offset in various directions from the center of the spoiled transmit beam. An example of four simultaneous receive beams in a cluster is shown in Figure 13.37. To search the same volume covered by this four beam cluster with a single beam radar would take approximately four times as long since the transmit and receive beams would need to be sequentially scanned to each beam position. Increasing the number of beams in the receive cluster, while also increasing the transmit beam spoiling by an equivalent amount, reduces the search frame time.

There is another technique for generating multiple simultaneous beams that does not use beam broadening on transmit. In this technique, each pulse in the waveform is divided into as many segments as there are beam positions. A pulse segment is transmitted sequentially in each of the desired beam positions, one transmit pulse right after the other. After all the pulses have been transmitted, multiple simultaneous receive beams are formed with a receive beam located in each of the transmit beam positions. In this method, each of the transmit beams has the full array gain. In order to have similar performance to the beam-broadening technique, the transmit pulse segment in each beam position would be $1/N$ times as long as the transmit pulse in the beam-broadened technique, where N is the number of simultaneous receive beams. In either case, it is necessary to trade energy for time in order to achieve the desired search frame time.

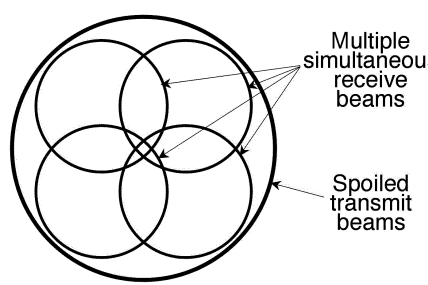

FIGURE 13.37 A spoiled transmit beam and a cluster of four simultaneous receive beams

A multiple simultaneous receive beam cluster can be formed in several different ways. If analog beamforming is used, the receive signals can be split N ways into N separate analog beamformers. Each analog beamformer is designed to produce one of the N offset beams in a beam cluster. Another way to generate multiple simultaneous receive beams is to use digital beamforming (DBF), which is discussed in more detail in the next section. DBF is usually preferred when a large number of beams are to be formed.

13.12 DIGITAL BEAMFORMING

Many phased array radars use analog beamforming. In an analog beamformer, the received signals from each element are combined at radio frequencies. At the output of the analog beamformer, centralized receivers downconvert the signal from radio frequency (RF) to an intermediate frequency (IF) and an analog-to-digital converter (ADC) is used to digitize the IF signal. In digital beamforming (DBF), the RF signals are digitized at either each individual element or each subarray. Once the signals have been digitized, various weighted combinations of the digitized signals can be used to form multiple simultaneous receive beams. Figure 13.38 shows array architectures for analog beamforming and DBF at the element and subarray level.

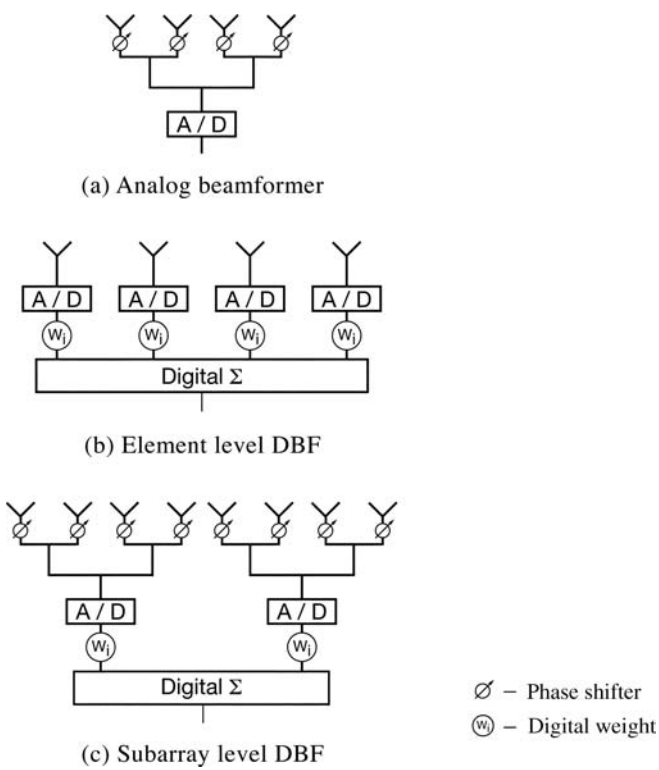

FIGURE 13.38 Array architectures for analog and digital beamforming

The benefits of DBF include improved dynamic range, faster search frame times if multiple simultaneous beams are used, and better control of amplitude and phase for adaptive nulling and lower sidelobe levels.

Shipboard radars had been designed to operate primarily in open ocean environments. However, the changing world will require shipboard radars to operate much closer to land. As a result, Navy radars must have significantly higher clutter rejection capabilities and larger dynamic ranges than existing radar systems. Recently, digital beamforming has been proposed for radar systems that must detect small RCS targets in severe clutter environments.[99]

The dynamic range determines the range of power levels that can be processed in the linear operating region of the receiver. The radar system must be able to process high power clutter returns without saturating the receiver. One reason DBF has been proposed for future radar is because DBF provides the radar system with a significantly higher dynamic range than can be achieved with analog beamforming, which has a centralized receiver. In a DBF architecture, there are N digital receivers, one at each of the N elements or subarrays. Therefore, the dynamic range of a DBF radar system has $10\log(N)$ higher dynamic range than an analog beamforming radar that utilizes the same receiver, provided the noise and distortion in each receiver are decorrelated among all receivers.[100]

DBF can be implemented at either the element level[101] or the subarray level. Element-level DBF requires a digital receiver, which consists of a downconverter and an ADC, at each element. Subarray-level DBF requires a digital receiver at each subarray. A fully digital array, which has DBF at the element level, allows for multiple, simultaneous independent beams. These independent beams can be steered in any direction. DBF at the subarray level can produce a multiple, simultaneous beam cluster located within the subarray pattern. DBF at the subarray level uses phase shifters at the element and an analog subarray beamformer, with a digital receiver located at the output of each subarray. Time delay steering can be achieved at the subarray level through the use of digital time delays. The multiple beam cluster is formed by digitally combining the subarrays to form simultaneous beams that are offset from one another. In practice, DBF is frequently implemented at the subarray level rather than the element level due to the size, weight, and high cost of digital receivers. Another practical advantage of subarray-level DBF is that less digital data, which must be processed to form the receive beams, is produced than for element-level DBF.

DBF can provide more efficient time-energy management than a single-beam analog beamforming array. Since DBF can produce multiple simultaneous beams, energy can be traded off for improved search frame times as was discussed in Section 13.11.

13.13 RADIATION PATTERN NULLING

Phased array antennas can be designed to have deterministic antenna patterns or adaptive antenna patterns. When no interfering signals are present, a phased array antenna with a deterministic antenna pattern will typically utilize phase weights that provide a linear phase front over the array face and amplitude weights that produce the desired sidelobe levels. The antenna performance can be characterized by parameters such as antenna beamwidth, gain, and peak and RMS sidelobe levels. Interfering radio frequency signals that are intentional, such as those produced by jammers, or unintentional, such as those produced by other radars or clutter, may significantly degrade the

performance of static-pattern phased array antennas. As a result, methods for placing nulls in the direction of the interference in the phased array radiation patterns have been the subject of much research.[102–105] Either deterministic radio frequency nulling or adaptive nulling can be used to place nulls in the antenna pattern in the direction of the interfering source.

If the location of the interfering source is stationary and the direction of the interferer is known, a deterministic RF null can be placed in the antenna pattern at that specific direction. Deterministic antenna patterns with nulls steered in specific directions can be achieved by modifying the weights at each element. These modified weights can be either the amplitude and phase of each element or only the phase of each element. Regardless of whether amplitude and phase nulling or phase-only nulling is used, the weights at each element are not time-varying for deterministic RF nulling. Array configurations for performing deterministic RF nulling using amplitude and phase weights and phase-only weights at each element are shown in Figure 13.39.

Deterministic RF nulling using amplitude and phase control at each element provides better performance than phase-only nulling. Deterministic RF nulling can be accomplished by using perturbation techniques to generate the weights at each element that will produce the antenna pattern with nulls.[102] With perturbation techniques, first the weights at each element are computed to generate the original antenna pattern without nulls. Then, the original weights are perturbed to produce nulls in the desired directions of the antenna pattern. The intent of the perturbation algorithm is to maximize the signal-to-interference-plus-noise ratio, while minimizing the deviation between the original element weights and the perturbed element weights.[104] Full amplitude and phase control at each element ensures that the perturbed antenna pattern has nulls in the desired directions with minimally perturbed weights.[102] However, phase-only control

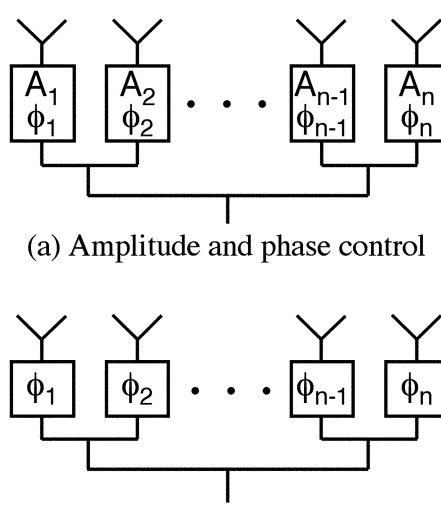

FIGURE 13.39 Array configurations for performing deterministic RF nulling: (*a*) amplitude and phase control at each element and (*b*) phase-only control at each element

at each element may result in situations where a solution does not exist.[102] An example of a deterministic antenna pattern with and without nulling is shown in Figure 13.40. The solid line in Figure 13.40 shows a deterministic antenna pattern at broadside for a 25-element linear array with $\lambda/2$ element spacing when no interference is present. Uniform illumination and no amplitude and phase errors were assumed. The dashed line in Figure 13.40 shows the antenna pattern for the same array when an interfering source is present at +21° and amplitude and phase weighting is used to steer a null in the pattern in the direction of the interfering source.

Radar systems can utilize deterministic RF nulling to place nulls in both the transmit and the receive antenna patterns. On transmit, nulls can be placed in the direction of high ground clutter to reduce the clutter power reflected back toward the antenna. Active arrays typically have both amplitude and phase control at each element, which allows either full amplitude and phase nulling or phase-only nulling to be used. However, when transmitting, it is desirable to have uniform illumination across the aperture to produce the highest aperture efficiency possible. Also, for active arrays, it is desirable to keep the high-power transmit amplifiers in saturation. Hence, when nulling on transmit, it is desirable to use phase-only nulling to maintain the aperture efficiency. On receive, amplitude weighting across the array is typically used to produce the desired sidelobe levels. Because this amplitude weighting produces a taper loss on receive, using full amplitude and phase control for nulling the radiation pattern is less of a concern than on transmit.

The incorporation of adaptive nulling into phased array antennas allows phased arrays to have adaptive antenna patterns on receive. Adaptive techniques are used to sense and automatically respond to a time-varying interference environment. The goal is to preserve the desired signal while simultaneously reducing unwanted interference. This real-time antenna pattern control is accomplished by adjusting the weights at each receiver to maximize signal-to-interference-plus-noise ratio. The amplitude and phase weight for the signal at each receiver is adaptively computed and implemented so that the desired signal combines coherently whereas the interference combines incoherently.

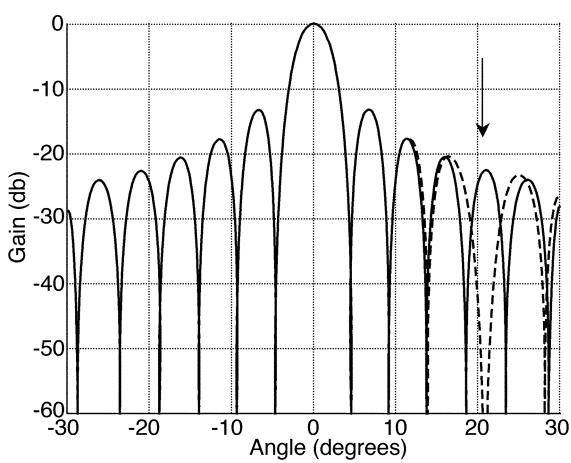

FIGURE 13.40 Deterministic antenna pattern with and without nulling for a 25-element linear array. Interfering source is located at +21 degrees.

Adaptive beamforming can be implemented by using auxiliary receivers in a sidelobe cancellation system or by using digital beamforming. In a DBF system, adaptive beamforming is accomplished either with the use of subarray receivers or with auxiliary receivers. If subarray receivers are used, the number of nulls that can be placed in the antenna pattern depends upon the number of degrees of freedom (DOF). For adaptive beamforming, the number of degrees of freedom is $N - 1$, where N is the number of receivers in the DBF array.[100] If adaptive beamforming is implemented using digital beamforming, element-level DBF will have significantly better performance than subarray-level DBF, because subarray-level DBF has far fewer degrees of freedom. However, element-level DBF is usually cost prohibitive except for arrays with a small number of elements. Hence, subarray-level DBF is frequently pursued because it requires far fewer digital receivers. However, subarrays are not the best choice of array architectures for a given number of DOF in an adaptive array. [106] In subarray DBF, the main beam of each subarray must be aligned with the main-beam direction of the array. When an interfering source is present in the sidelobe region, the subarray-level DBF architecture does a poor job of sensing this interfering signal because the subarray gain is low in the sidelobe region.[106]

13.14 CALIBRATION OF ACTIVE PHASED ARRAY ANTENNAS

Active phased array antennas must be calibrated in order to ensure that the radiation pattern of the antenna meets the antenna performance specifications. Antenna characteristics such as sidelobe level and main-beam gain are typically specified, but these specifications can be translated into allowable amplitude and phase errors at each element.

Calibration can be divided into two categories: factory calibration and in-the-field calibration.[107] Factory calibration is only performed once, usually at the antenna test range of the phased array manufacturer. In-the-field calibration is performed at regular intervals throughout the life of the array, after it has been deployed. The antenna measurements required for factory calibration can be made in three different types of antenna ranges: near field, compact, or far field. For large ground-based or shipboard phased arrays, factory calibration is usually performed using a planar near-field antenna measurement facility.[108,109] An attractive feature of the near-field range is that the amplitude and phase of each element can be measured and a full hemispheric antenna pattern can be generated. Near-field ranges are suitable for measuring low-sidelobe, high-gain antennas.[110]

Planar near-field antenna measurements are made by scanning a probe in a plane parallel to the antenna under test and measuring the amplitude and phase at each probe location. In rectangular coordinates, the probe position is given by (x,y,z). During the scanning, the x and y coordinates of the probe are varied and the distance of the scanning plane from the antenna under test is kept constant at z_o. The value of z_o is typically a little more than three wavelengths. The phase front should be sampled with probe positions that satisfy the Nyquist sampling theorem, which yields a maximum sampling distance between points in the x-y plane of $\Delta x = \Delta y = \lambda/2$. In practice, the active array elements are turned on one at a time in coordination with the probe position. Some examples of existing systems that use near-field ranges to perform factory calibration are THAAD and SAMPSON.[108,109]

For an active array, both the phase and amplitude of each element must be measured in order to determine the correction constants for each array element in both transmit and receive mode. Full calibration of an active array is measurement intensive. It is common for phase shifters and attenuators to each have as many as 7 bits or 128 different states. In addition, active components should be characterized at several frequencies in the operating frequency band and over several temperatures. As a result, thousands of measurements are required to fully characterize the performance of each element. Not all states need to be measured for each element, but eliminating measurements at some of the states will cause the calibrated amplitude and phase errors to increase.[108]

Phase shifters usually exhibit small variations in amplitude over phase states, whereas attenuators exhibit large variations in-phase over gain states. Therefore, it is desirable to calibrate the attenuator first. The phase shifter can then be calibrated without changing the attenuator setting.[108] Once the characteristics of each T/R channel are measured, correction factors are calculated and stored for future use. The appropriate correction factors are applied to bring the antenna into calibration for a given mode of radar operation.

Once the active phased array is fielded, in-the-field calibration must be performed to keep the antenna within specifications. Active components drift over time and these aging effects require calibration to be performed in the field. A number of different techniques have been proposed for in-the-field calibration including mutual coupling,[111] near-field antennas,[109] and RF sampling.

Mutual-coupling techniques utilize the mutual coupling paths between adjacent array elements for transmission of calibration signals (see Figure 13.41*a*). In this technique, a signal is transmitted from an array element, and the nearest elements surrounding the transmit element are used to receive the transmitted calibration signal.[111] The signal received is compared to a stored reference obtained during factory tests. Only one element transmits at a given time, and this procedure is repeated until all the elements are measured. Calibration using mutual coupling can be interspersed with normal radar operating modes and requires only a small fraction of the available radar resources.

Another technique to perform in-the-field calibration uses radiators placed in the near field around the periphery of the array (see Figure 13.41*b*). These additional radiators are dedicated to the calibration of the active array. To calibrate the array in receive mode, test signals are routed to each of the radiators used for calibration.[109] The signal received from a T/R module is compared to a stored reference obtained during factory test.

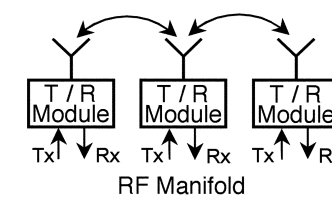

(a) Mutual coupling

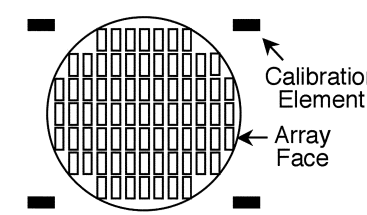

(b) Near-field antennas

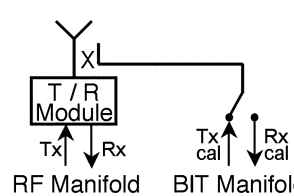

(c) RF sampling

FIGURE 13.41 Active array calibration techniques: (*a*) mutual coupling, (*b*) near-field antennas, and (*c*) RF sampling

The calibration constants are then modified in order to restore the antenna so its calibration is as close as possible to the original factory calibration. This technique requires several additional transmit and receive hardware channels to be dedicated for in-the-field calibration.

RF sampling can also be used to calibrate an active phased array (see Figure 13.41*c*). The RF sampling technique uses built-in calibration circuitry in the array to inject a calibration signal between the T/R module and the radiator. This technique can be used to measure RF output power, receive gain, and phase and attenuation bit accuracy. These measured values are then compared with reference values. A major disadvantage of this technique is that it requires significant additional hardware, including a separate built-in test (BIT) manifold. Also, the calibration path does not include the radiator.

13.15 PHASED ARRAY SYSTEMS

A number of phased array radar systems have been built,[112] and a representative selection is briefly reviewed below.

Lockheed Martin Corporation Phased Array Radars. (*Courtesy of Lockheed Martin Corporation*)

AN/SPY-1.[113,114] This S-band phased array radar is part of the Navy Aegis weapon system and was developed by RCA, now Lockheed Martin. It has four phased array apertures to give unobstructed hemispherical coverage (Figure 13.1). In its early configuration, it used a simple feed system with, on receive, 68 subarrays, each containing 64 waveguide-type radiators for a total of 4352 elements. On transmit, subarrays were combined in pairs, and 32 such pairs gave a transmit aperture of 4096 radiators. The phase shifters fed directly into waveguide radiators, had 5 bits, and were of the nonreciprocal, latching garnet configuration. A later version was designed for low sidelobes. The subarray size had to be reduced to 2 elements to avoid quantization lobes, and similarly, the phase shifter had to be refined by driving it with 7-bit accuracy. The resulting phased array has an aperture with a constrained-feed structure and 4350 waveguide-type radiators. Monopulse sum and difference receive patterns and the transmit pattern are separately optimized.

COBRA. The COunter Battery RAdar (COBRA) C-Band solid -state phased array radar (see Figure 13.42) locates rocket launchers, artillery batteries, mortars, shell impact points, and jamming directions. The antenna, which is mechanically trained, has 2720 radiating elements, each fed by a solid state T/R module to provide wide electronic scan coverage. It is produced by Euro-Art GmbH, a consortium of Lockheed Martin MS2 (Moorestown, NJ), EADS Deutschland (Unterschleissheim, Germany), Thales Air Defence (Bagneux, France), and Thales UK, Limited (Crawley, West Sussex, England), for the Ministries of Defence of France, Germany, and the United Kingdom.

Volume Search Radar. The S-band Volume Search Radar (VSR) phased array (see Figure 13.43) provides search and AAW capability to the Dual Band Radar System for DD(X). It has 2688 radiating elements with a T/R module per element. Although the active radiating aperture is approximately circular, the corners have been filled in

FIGURE 13.42 COBRA phased array mounted on radar system vehicle (*Courtesy of Lockheed Martin Corporation*)

with terminated elements to form a rectangular aperture for purposes of minimizing antenna radar cross section. All active components are accessible from the rear for ease of maintenance aboard ship.

Ground-Based Radars (AN/TPS-59, AN/FPS-117, and AN/TPS-77). Lockheed Martin's long-range, solid-state 3D radar systems (see Figure 13.44) operate at L band between 1.2–1.4 GHz. These systems provide position data for en-route tracking of commercial aircraft, air surveillance/air defense, navigational assistance, tactical control, and tactical ballistic missile (TBM) defense. The AN/TPS-59 was the world's first totally solid-state antenna/array. The AN/FPS-117 was developed shortly thereafter and is typically installed and operated at a fixed site, but it can also be configured on a trailer for deployment. The AN/TPS-77 is a mobile/transportable series of solid-state radar systems. Each system incorporates primary surveillance radar, secondary surveillance radar (IFF), command and control display consoles, communications equipment, various options, and transport configurations customized for each customer's specific mission.

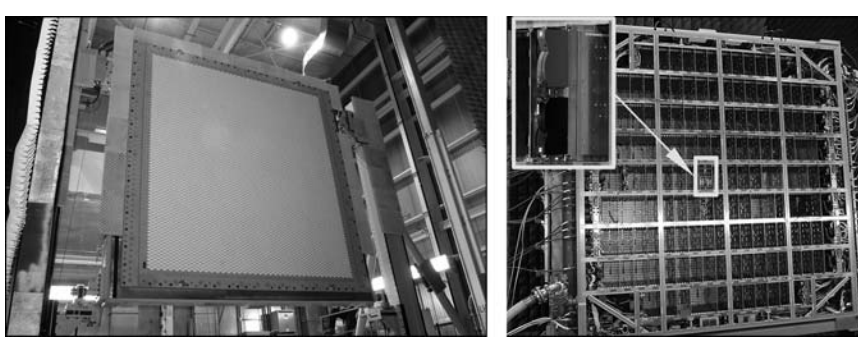

FIGURE 13.43 Front (left) and rear views of Volume Search Radar S-Band engineering development model active phased array mounted in near-field test facility during assembly. Rear view shows detail of easily replaceable lowest replaceable units. (*Courtesy of Lockheed Martin Corporation*)

AN/TPS-59

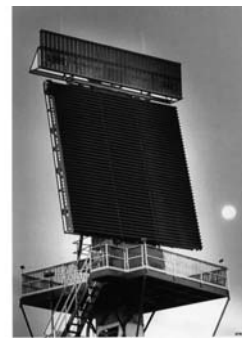

AN/FPS-117

AN/TPS-77

FIGURE 13.44 Ground-based radar system configurations (*Courtesy of Lockheed Martin Corporation*)

The main feature of these systems is the planar phased array, which has modular construction with distributed all-solid-state electronics, including RF power generation and electronic steering in the elevation axis. Antenna rotation for the system is at 5, 6 or 10, 12 revolutions per minute (rpm), providing 360° azimuth coverage while electronically step-scanning in elevation. It provides full performance over a nominal 20° in the elevation plane to an altitude of 100,000 feet and up to 60° in elevation during TBM tracking. The antenna/array incorporates monopulse radar techniques. These techniques allow accurate target angular position, using three data channels—sum, delta azimuth (AZ), and delta elevation (EL)—within the array and the data-processing group.

The data-processing group applies moving target indicator (MTI) and doppler processing to the receive signal to produce subclutter visibility for target detection. Selection of the operating frequency is dependent upon the radar's mode of operation and the frequency options selected by the operator. The antenna/array shown in Figure 13.44 is constructed of either 54 (AN/TPS-59), 44 (AN/FPS-117), or 34 (AN/TPS-77) identical horizontal passive row-feed networks, one above another on 6.6-inch centers. Mounted directly behind each row feed is a dedicated row transmitter and receiver. The row transmitters and receivers are similar for each row. They perform all the RF functions, including RF power generation, phase shifting to steer the antenna beam in elevation, and receive preamplification to provide a low-noise figure. The RF power is generated by direct amplification through modular solid-state power amplifiers in the row transmitters. The energy from these power modules is combined within the row transmitter, which drives the row feed. The RF energy from the row feeds is combined in space to form the radiated beam. Unlike a tube transmitter, which operates at high peak power and low duty factor, the power modules operate at low peak power and high duty factors (10% to 20%). Long-duration pulses are transmitted and then compressed during receive to obtain the required range resolution. A performance margin is built in to the radar system to allow for field degradation of the distributed array components between scheduled maintenance periods. Since array component failures induce only a gradual degradation, maintenance can be performed on a planned basis. Online system sensitivity and performance level is checked and displayed by the performance monitoring and fault isolation (MFI) function.

These long-range, three-dimensional air-surveillance radars provide an off-the-shelf solution to primary air-surveillance needs. They have been designed for remote operation in harsh environments, and with their established logistics support, built-in performance monitoring and fault isolation, high reliability, and worldwide investment, these systems have an inherent low cost of ownership.

Northrop Grumman Corporation Phased Array Radars. (*Courtesy of Northrop Grumman Corporation*)

AWACS (Airborne Warning and Control System).[13,14,115] The Airborne Warning and Control System (AWACS) provides all-weather long-range surveillance, command, control, and communications. The phased array antenna is a 26 ft by 4.5 ft elliptically shaped, ultra-low sidelobe array, consisting of 28 slotted waveguides with over 4000 slots (see Figure 13.45). Mounted atop the aircraft fuselage in a rotating dome, the S-band antenna scans mechanically over 360° in azimuth, and scans electronically in elevation through 28 reciprocal beam-steering phase shifters. In addition, 28 nonreciprocal beam offset phase shifters provide offset of the receive beam from the transmit beam during elevation scanning to compensate for time delay between transmit and receive of long-range aircraft returns. The Radar System Improvement Program (RSIP) provides the most significant upgrade to the AWACS radar since its development in the early 1970s. RSIP introduces new waveforms and processing, providing improvements in detection range, angular accuracy, as well as range and angular resolution.

AN/TPS-78. The AN/TPS-78 is an update to the AN/TPS-70/75 S-band, three-dimensional tactical radar family developed by the Northrop Grumman Corporation (Figure 13.46). The AN/TPS-78 planar array shown in Figure 13.46 exhibits very low

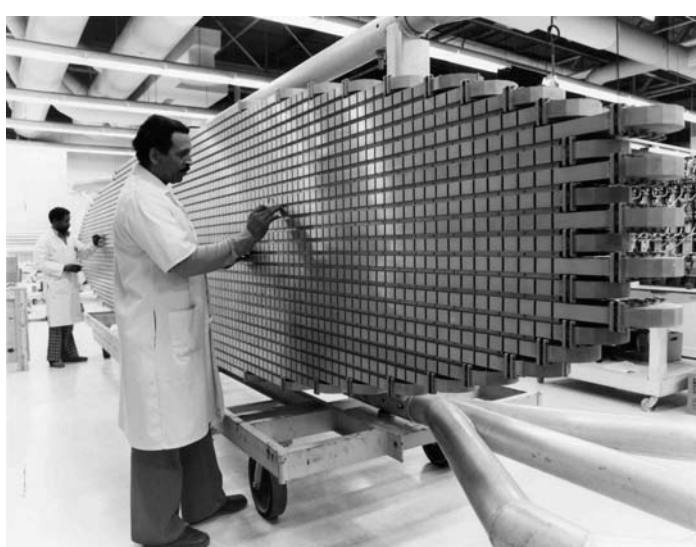

FIGURE 13.45 AWACS antenna (*Courtesy of Northrop Grumman Corporation*)

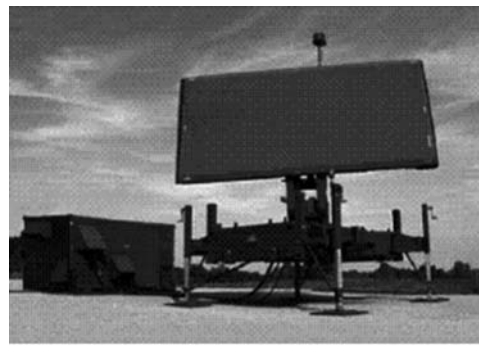

FIGURE 13.46 AN/TPS-78 antenna (*Courtesy of Northrop Grumman Corporation*)

azimuth sidelobes. The array is a slotted waveguide design of 36 sticks and 94 horizontally polarized slots per stick. The array is fed from a solid-state transmitter and transmits a single fan beam in elevation optimized for maximum gain at low altitudes. On receive, the array output is combined into six simultaneous narrow elevation beams that cover from 0 to 20°. Each receive beam is processed in a digital receiver. Accurate height information is extracted using amplitude monopulse techniques by comparing receive energy in adjacent beams. A narrow azimuth beamwidth on transmit and receive and stacked receive beams provide good radar angle resolution. Azimuth coverage of 360° is achieved by rotating the array at a nominal surveillance rate.

A unique feature of the AN/TPS-78 array is that the array has an integral low sidelobe IFF array embedded in the array face. This not only provides excellent registration between radar and IFF returns, but also supports fast setup and teardown time for transporting the radar in its mobile configuration.

Joint STARS Antenna. The Joint Surveillance Target Attack Radar System (Joint STARS) provides long-range airborne surveillance and tracking of stationary and moving ground targets (see Figure 13.47). The phased array antenna for this system is a 24-ft wide by 2-ft high planar X-band slotted array. It is mounted inside a radome underneath the fuselage of an E-8A aircraft and can be mechanically rotated ±100° in elevation for operation looking out either side of the aircraft. The system operates in a synthetic aperture radar (SAR) mapping mode as well as in a three-port azimuth interferometer ground moving target indication (GMTI) target detection and tracking mode. Use of the three-port aperture on receive enables a clutter suppression interferometry technique that allows the operator to detect, accurately locate, and track slow moving ground targets in the presence of competing ground clutter.

Raytheon Company Phased Array Radars. (*Courtesy of Raytheon Company*)

PATRIOT.[116] The PATRIOT is a multifunction phased array radar system developed by Raytheon for the Army in the form of a lens using an optical feed, as shown previously in Figure 13.30. Sum and difference patterns are separately optimized with a monopulse feed. The aperture is round and contains approximately 5000 elements.

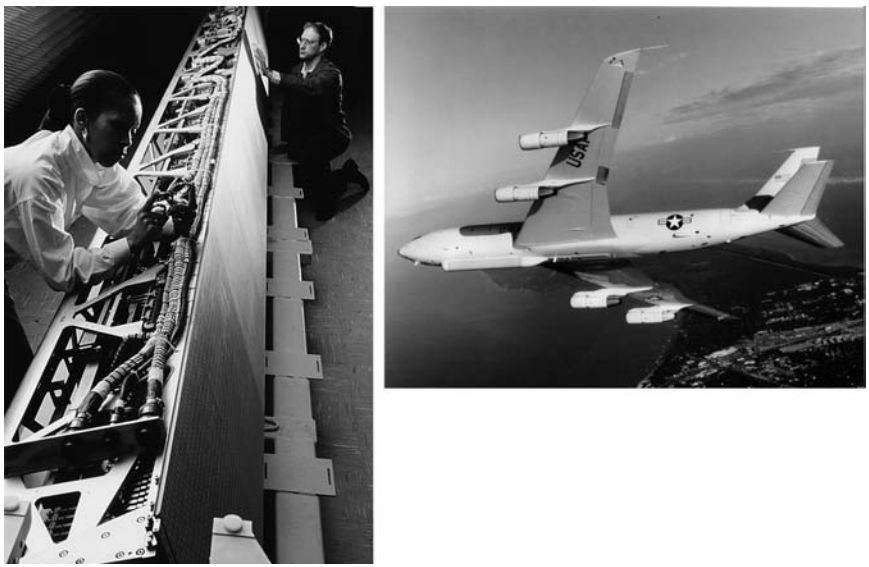

FIGURE 13.47 Joint STARS antenna and aircraft (*Courtesy of Northrop Grumman Corporation*)

It uses 4-bit flux-driven nonreciprocal ferrite phase shifters and waveguide-type radiators at both apertures. The antenna is shown in Figure 13.48. It is mounted on a vehicle and folds flat for transportation.

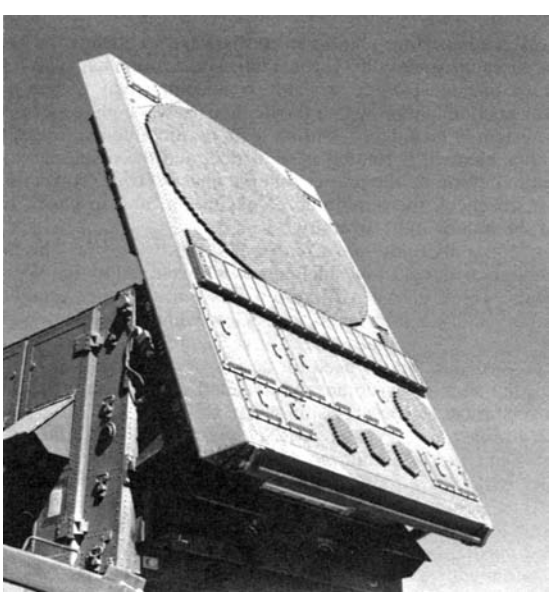

FIGURE 13.48 PATRIOT multifunction phased array (*Courtesy of Raytheon Company*)

Terminal High Altitude Area Defense (THAAD). THAAD is a ground-based system designed to destroy the theater ballistic missile threats to troops, military assets, and allied territories. THAAD consists of a hit-to-kill missile, radar, launcher, and Battle Management/Command, Control, and Communications (BMC3) system.

The THAAD radar (see Figure 13.49) is an X-band, phased array, solid-state radar capable of search, threat detection, classification, and precision tracking at long ranges. The radar design delivers high power output and beam/waveform agility in order to support the long-range functional requirements of the THAAD mission. The THAAD element components work in concert to detect, assign, and destroy incoming short- to medium-range ballistic missiles by providing the firing battery with target acquisition, interceptor support, and intercept assessment functions. These functions include surveillance, THAAD missile track, in-flight data uplink/downlink, target classification/typing/identification, and intercept assessment.

The single face phased-array radar is 12.5 m long, mounted on a Heavy Expanded Mobile Tactical Truck and capable of being transported in a C-130 Hercules aircraft. The radar is nonrotating and has a 120º field of view. The radar uses its 9.2 m^2 full field-of-view phased array aperture to acquire theater missile threats at a range of up to 1,000 km. This radar uses 25,344 X-band solid-state transmit/receive modules in the phased array.

X-Band Radar (XBR). The nine-story-high XBR is the world's largest X-band radar, weighing four million pounds (see Figure 13.50). The SBX platform that it sits on stands more than 250 ft tall and displaces more than 50,000 tons. It consists of a semi-submersible oil production platform, topped with the XBR. XBR is the primary payload on the semi-submersible platform supporting the Ground-Based Midcourse Defense (GMD) phase of the Missile Defense Agency (MDA) Ballistic Missile Defense System (BMDS). SBX's floating platform, a modified oil-drilling vessel, was designed for

FIGURE 13.49 THAAD radar (*Courtesy of Raytheon Company*)

FIGURE 13.50 SBX—over 250 ft tall and displacing more than 50,000 tons (*Courtesy of Raytheon Company*)

exceptional stability in high winds and storms. Measuring 240 ft wide and 390 ft long, the vessel includes a power plant, bridge and control rooms, living quarters, storage areas, and enough floor space and infrastructure to support the X-band radar.

The X-band radar itself, which sits on top of the floating platform, is the largest, most sophisticated phased array, electro-mechanically steered X-band radar in the world. It consists of thousands of elements driven by transmit/receive (T/R) modules. In the X-band radar, they will provide the full fire control sensor functions for the Ground-Based Midcourse Defense system, including search, acquisition, tracking, discrimination, and kill assessment.

SPY-3. The AN/SPY-3 Multi-Function Radar (MFR) is the U.S. Navy's first shipboard active phased array multifunction radar. It is an X-band active phased array radar designed to meet all horizon search and fire control requirements for the Navy. MFR is designed to detect low-observable anti-ship cruise missile (ASCM) threats and support fire-control illumination requirements for multiple missiles. MFR combines the functions provided by several separate radars aboard Navy combatant ships and also supports new ship-design requirements for reduced radar cross section and significantly reduced manning (no operators).

The radar performs such functions as horizon search, limited above-the-horizon search, and fire control track and illumination. One of the most significant design features of the radar is to provide automatic detection, tracking, and illumination of low-altitude threat missiles in the adverse environmental conditions routinely found in coastal waters.

SPY-3 uses three fixed-face arrays, each containing around 5,000 transmit/receive (T/R) elements (see Figure 13.51). These elements are connected to T/R integrated multi-channel modules, each of which drives eight elements. Individual modules are designed to slide into the array structure and provide a high-conductivity thermal path to the cooling-array manifold without having any connection to the T/R module itself.

FIGURE 13.51 AN/SPY-3 Multi-Function Radar (*Courtesy of Raytheon Company*)

REFERENCES

1. A. Blondel, "Improvements in or relating to radiator systems for wireless telegraphy," Belgian Patent 163,516, 1902; British Patent 11, 427, 1903.
2. S. G. Brown, "Improvements in wireless telegraphy," British Patent 14,449, 1899.
3. R. M. Foster, "Directive diagrams of antenna arrays," *Bell System Tech. J.*, vol. 5, pp. 292–307, April 1926.
4. R. C. Hansen, *Microwave Scanning Antennas*, Vols. I, II, and III, New York: Academic Press, 1964.
5. N. Amitay, R. C. Pecina, and C. P. Wu, "Radiation properties of large planar arrays," *Bell Teleph. Syst. Monog*., 5047, February 1965.
6. A. A. Oliner and G. H. Knittel, *Phased Array Antennas*, Norwood, MA: Artech House, 1972.
7. L. I. Stark, "Microwave theory of phased array antennas—A Review," *Proc. IEEE*, vol. 62, pp. 1661–1701, December 1974.
8. R. J. Mailloux, "Phased array theory and technology," *Proc. IEEE*, vol. 70, March 1982.
9. A. W. Rudge, K. Milne, A. D. Olver, and P. Knight, *The Handbook of Antenna Design*, Vol. 2, London: Peter Peregrinus, Ltd., 1983.
10. R. C. Johnson and H. Jasik (eds.), *Antenna Engineering Handbook*, 2nd Ed., New York: McGraw-Hill Book Company, 1984.
11. E. Brookner, "Phased array radars," *Sci. Am*., vol. 252, pp. 94–102, February 1985.
12. H. P. Steyskal, "Phased arrays 1985 symposium," in *RADC Rept. TR*-85-171, Rome Air Development Center, Bedford, MA, August 1985.
13. E. Brookner, "A review of array radars," *Microwave J*., vol. 24, pp. 25–114, October 1981.
14. E. Brookner, "Radar of the 80's and beyond," *IEEE Electro 84*, May 1984.

15. E. Brookner, "Array radars: An update," *Microwave J.*, vol. 30, pt. I, pp. 117–138, February 1987; pt. II, pp. 167–174, March 1987.
16. W. A. Harmening, "A laser-based, near-field probe position measurement system," *Microwave J.*, pp. 91–102, October 1983.
17. R. J. Mailloux, Chapter 21 in *Antenna Engineering Handbook*, R. C. Johnson and H. Jasik (eds.), 2nd ed., New York: McGraw-Hill Book Company, 1984.
18. G. V. Borgiotti, Chapter 11 in *The Handbook of Antenna Design*, A. W. Rudge, K. Milne, A. D. Olver and P. Knight (eds.), vol. 2, London: Peter Peregrinus, Ltd., 1983.
19. K. G. Schroeder, "Near optimum beam patterns for phase monopulse arrays," *Microwaves*, pp. 18–27, March 1963.
20. J. Frank, "Phased array antenna development," Johns Hopkins University, Appl. Phys. Lab. Rept. TG 882, pp. 114–117, March 1967.
21. W. E. Scharfman and G. August, "Pattern measurements of phased arrayed antennas by focussing into the near zone," in "Phased Array Antennas," A. A. Oliner and G. H. Knittel (eds.), Norwood, MA: Artech House, 1972, pp. 344–349.
22. D. K. Alexander and R. P. Gray, Jr., "Computer-aided fault determination for an advanced phased array antenna," presented at Proc. Antenna Application Symp., Allerton, IL., September 1979.
23. J. Ronen and R. H. Clarke, "Monitoring techniques for phased-array antennas," *IEEE Trans.*, vol. AP-33, pp. 1313–1327, December 1985.
24. R. H. Collings, "Current sheet antenna," U.S. Patent 3,680,136, 1972.
25. A. A. Oliner and R. G. Malech, Chapters 2–4 in *Microwave Scanning Antennas*, R. C. Hansen, vol. III, New York: Academic Press, 1964.
26. L. I. Parad and R. W. Kreutel, "Mutual effects between circularly polarized elements," in *Symp. USAF Antenna Res. Develop., Antenna Arrays Sec., Abstr.*, University of Illinois, Urbana, 1962.
27. M. I. Skolnik, *Introduction to Radar Systems*, 2nd Ed., New York: McGraw-Hill Book Company, 1980, pp. 504–506.
28. J. M. Howell, "Limited scan antennas," presented at IEEE AP-5 Int. Symp., 1972.
29. J. S. Ajioka, "Frequency-scan antennas," *Antenna Engineering Handbook*, Chap. 19, R. C. Johnson and H. Jasik (eds.), 2nd Ed., New York: McGraw-Hill Book Company, 1984.
30. W. F. Gabriel, Guest editor, special issue on adaptive antennas, *IEEE Trans.*, vol. AP-24, September 1976.
31. J. R. Forrest, Guest editor, special issue on phased arrays, *Proc. IEE* (*London*), vol. 127, pt. F, August 1980.
32. H. Steyskal, "Digital beamforming antennas—an introduction," *Microwave J.*, vol. 30, pp. 107–124, January 1987.
33. J. L. Allen, "A theoretical limitation on the formation of lossless multiple beams in linear arrays," *IRE Trans.*, vol. AP-9, pp. 350–352, July 1961.
34. J. Blass, "The multidirectional antenna: A new approach to stacked beams," in *IRE Int. Conv. Rec.*, vol. 8 pt. 1, 1960, pp. 48–50.
35. H. Gent, The bootlace aerial, *Royal Radar Estab. J.* (*U.K.*), pp. 47–57, October 1957.
36. W. Rotman and R. F. Turner, "Wide angle microwave lens for line source application," *IEEE Trans.*, vol. AP-11, pp. 623–632, November 1963.
37. S. A. Schelkunoff, "A mathematical theory of linear arrays," *Bell, Syst. Tech. J.*, vol. 22, pp. 80–107, January 1943.
38. J. F. Ramsay, J. P. Thompson, and W. D. White, "Polarization tracking of antennas," presented at IRE Int. Conv., Session 8, Antennas I, 1962.
39. P. M. Woodward, A method of calculating the field over a planar aperture required to produce a given polar diagram, *J. IEE* (*London*), vol. 93, pt. 3A, pp. 1554–1558, 1946.
40. R. C. Hansen, "Aperture theory," in *Microwave Scanning Antennas*, vol. I, New York: Academic Press, pp. 18–21.
41. J. F. Ramsay, "Lambda functions describe antenna diffraction pattern," *Microwaves*, pp. 70–107, June 1967.

42. A. Ksienski, "Equivalence between continuous and discrete radiating arrays," *Can. J. Phys*., vol. 39, pp. 35–349, 1961.
43. W. H. Von Aulock, "Properties of phased array," *IRE Trans*. Vol. AP-9, pp. 1715–1727, October 1960.
44. E. D. Sharp," Triangular arrangement of planar-array elements that reduces number needed," *IRE Trans*., vol. AP-9, pp. 126–129, March 1961.
45. J. L. Allen et al., "Phased array radar studies," MIT Lincoln Lab. Tech. Rept. 381, March 1965.
46. J. L. Allen and B. L. Diamond, "Mutual coupling in array antennas," MIT Lincoln Lab. Tech. Rept. 424, October 1966.
47. R. W. Bickmore, "Note on effective aperture of electrically scanned arrays," *IRE Trans*., vol. AP-6, pp. 194–196, April 1958.
48. B. L. Diamond, Chapter 3 in *Mutual Coupling in Array Antennas*, J. L. Allen and B. L. Diamond (eds.), MIT Lincoln Lab. Tech. Rept. 424, pt. III, October 1966.
49. J. Frank, "Phased array antenna development," *Johns Hopkins University, Appl. Phys. Lab. Rept. TG* 882, March 1967.
50. P. W. Hannan, "Element-gain paradox for a phased-array antenna," *IEEE Trans*., vol. AP-12, pp. 423–43, July 1964.
51. W. Wasylkiwskyj and W. K. Kahn, "Element patterns and active reflection coefficient in uniform phased arrays," *IEEE Trans*., vol. AP-22, March 1974.
52. W. Wasylkiwskyj and W. K. Kahn, "Element pattern bounds in uniform phased arrays." *IEEE Trans*., vol. AP-25, September 1977.
53. W. K. Kahn, "Impedance-match and element-pattern constraints for finite arrays," *IEEE Trans*., vol. AP-25, November 1977.
54. R. E. Willey, "Space tapering of linear and planar arrays," *IRE Trans*., vol. AP-10, pp. 369–377, July 1962.
55. H. A. Wheeler, "Simple relations derived from a phased-array antenna made of an infinite current sheet," *IEEE Trans*., vol. AP-13, pp. 506–514, July 1965.
56. J. L. Allen, "On array element impedance variation with spacing," *IEEE Trans*., vol. AP-12, p. 371, May 1964.
57. P. W. Hannan, "The ultimate decay of mutual coupling in a planar array antenna," *IEEE Trans*., vol. AP-14, pp. 246–248, March 1966.
58. T. T. Debski and P. W. Hannan, "Complex mutual coupling measured in a large phased array antenna," *Microwave J*., pp. 93–96, June 1965.
59. P. W. Hannan and M. A. Balfour, "Simulation of a phased-array antenna in a waveguide," *IEEE Trans*., vol. AP-13, pp. 342–353, May 1965.
60. B. L. Diamond, "Small Arrays—Their analysis and their use for the design of array elements," in *Phased Array Antennas*, A. A. Oliner and G. H. Knittel (eds.), Norwood, MA: Artech House,1972.
61. C. E. Grove, D. J. Martin, and C. Pepe, "Active impedance effects in low sidelobe and ultra wideband phased arrays," *Proc. Phased Arrays Symp*., 1985, pp. 187–206.
62. G. E. Evans and H. E. Schrank, "Low sidelobe radar antennas," *Microwave J*., pp. 109–117, July 1983.
63. G. E. Evans and S. G. Winchell, "A wide band, ultralow sidelobe antenna," presented at Antenna Applications Symp., Allerton, IL, September 1979.
64. S. G. Winchell and D. Davis, "Near field blockage of an ultralow sidelobe antenna," *IEEE Trans*., vol. AP-28, pp. 451–459, July 1980.
65. D. K. Barton and H. R. Ward, *Handbook of Radar Measurement*, Englewood Cliffs, NJ: Prentice-Hall, 1969, pp. 242–338.
66. J. F. Ramsey, "Lambda functions describe antenna/diffraction patterns," *Microwaves*, p. 60, June 1967.
67. W. M. Yarnall, "Twenty-seven design aids for antennas, propagation effects and systems planning," *Microwaves*, pp. 47–73, May 1965.

68. F. J. Harris, "On the use of windows for harmonic analysis with the discrete Fourier transform," *Proc. IEEE*, vol. 66, pp. 51–83, January 1978.
69. T. T. Taylor, "Design of line source antennas for narrow beamwidth and low sidelobes," *IEEE Trans*., vol. AP-3, pp. 16–28, 1955.
70. T. T. Taylor, "Design of circular apertures for narrow beamwidth and low sidelobes," *IEEE Trans*., vol. AP-8, pp. 17–22, 1960.
71. E. T. Bayliss, "Design of monopulse antenna difference patterns with low sidelobes," *Bell Syst. Tech. J*., pp. 623–650, May–June 1968.
72. D. K. Barton and H. R. Ward, *Handbook of Radar Measurement*, Englewood Cliffs, NJ: Prentice-Hall, 1969, pp. 256–266.
73. J. L. Allen, "The theory of array antennas," MIT Lincoln Lab. Rept. 323, July 1963.
74. J. Ruze, "Physical limitations on antennas," MIT Res. Lab. Electron. Tech. Rept. 248, October 30, 1952.
75. T. C. Cheston, "Effect of random errors on sidelobes of phased arrays," *IEEE APS Newsletter—Antenna Designer's Notebook*, pp. 20–21, April 1985.
76. J. Frank and J. Ruze, "Steering increments for antisymmetrically phased arrays," *IEEE Trans*., vol. AP-15, pp. 820–821, November 1967.
77. J. Brown (Private communication), 1951.
78. C. J. Miller, "Minimizing the effects of phase quantization errors in an electronically scanned array," in *Proc. Symp. Electronically Scanned Array Techniques and Applications*, RADC-TDR-64-225, vol. 1, 1964, pp. 17–38.
79. J. Frank, "Bandwidth criteria for phased array antennas," in *Phased Array Antennas*, A. A. Oliner and G. H. Knittel, Norwood, MA: Artech House, 1972, pp. 243–253.
80. W. B. Adams, "Phased array radar performance with wideband signals," *AES Conv. Rec*., November 1967, pp. 257–271.
81. C. B. Sharp and R. B. Crane, "Optimization of linear arrays for broadband signals," *IEEE Trans*., vol. AP-14, pp. 422–427, July 1966.
82. C. Rothenberg and L. Schwartzman, "Phased array signal bandwidth," IN *IEEE Int. Symp. Antennas Propag. Dig*., December 1969, pp. 116–123.
83. W. Rotman and R. F. Turner, "Wide angle lens for line source applications," *IEEE Trans*., vol. AP-11, pp. 623–632, 1963.
84. J. Blass, "The multi-directional antenna: a new approach to stacked beams," in *Proc. IRE Conv*., vol. 8, pt. I, 1960, pp. 48–51.
85. R. F. Kinsey and A. Horvath, "Transient response of center-series fed array antennas," in *Phased Array Antennas*, A. A. Olinerand and G. H. Knittel (eds.), Norwood, MA: Artech House, 1972, pp. 261–271.
86. A. R. Lopez, "Monopulse networks for series feeding an array antenna," in *IEEE Int. Symp. Antennas Propag. Dig*., 1967.
87. L. Stark, R. W. Burns, and W. P. Clark, Chapter 12 in *Radar Handbook*, M. I. Skolnik (ed.), 1st Ed., New York: McGraw-Hill Book Company, 1970.
88. J. F. White, *Semiconductor Control*, Norwood, MA: Artech House, 1977.
89. W. J. Ince, "Recent advances in diode and phase shifter technology for phased array radars," pts. I and II, *Microwave J*., vol. 15, no. 9, pp. 36–46, and no. 10, pp. 31–36, 1972.
90. J. F. White, "Diode phase shifters for array antennas," *IEEE Trans*., vol. MTT-22, pp. 658–674, June 1974.
91. M. A. Fruchaft and L. M. Silber, "Use of Microwave ferrite toroids to eliminate external magnets and reduce switching power," *Proc. IRE*, vol. 46, p. 1538, August 1958.
92. J. Frank, C. A. Shipley, and J. H. Kuck, "Latching ferrite phase shifter for phased arrays," *Microwave J*., pp. 97–102, March 1967.
93. W. J. Ince and D. H. Temme, "Phase shifters and time delay elements," in *Advances in Microwaves*, vol. 4, New York: Academic Press, 1969.

94. L. R. Whicker and C. W. Young, "The evolution of ferrite control components," *Microwave J.*, vol. 2, no. 11, pp. 33–37, 1978.
95. J. DiBartolo, W. J. Ince, and D. H. Temme, "A solid state 'flux drive' control circuit for latching-ferrite-phase shifter applications," *Microwave J.*, vol. 15, pp. 59–64, September 1972.
96. R. A. Pucel (ed.), *Monolithic Microwave Integrated Circuits*, New York: IEEE Press, 1985.
97. J. L. Poirier, "An analysis of simplified feed architectures for MMIC T/R module arrays," *Rome Air Development Center Rept. RADC-TR*-86-236 (AD A185474), February 1987.
98. W. H. Perkins and T. A. Midford, "MMIC technology: better performance at affordable cost," *Microwave J.*, vol. 31, pp. 135–143, April 1988.
99. B. Cantrell, J. de Graaf, F. Willwerth, G. Meurer, L. Leibowitz, C. Parris, and R. Stapleton, "Development of a digital array radar," *IEEE AEES Systems Magazine*, pp. 22–27, March 2002.
100. H. Steyskal, "Digital beamforming antennas: an introduction," *Microwave J.*, pp. 107–124, January 1987.
101. R. C. Hansen, *Phased Array Antennas*, New York: John Wiley & Sons, 1998.
102. H. Steyskal, R. A. Shore, and R. L. Haupt, "Methods for null control and their effects on the radiation pattern," *IEEE Trans. Antennas and Propagation*, vol. AP-34, no. 3, pp. 404–409, March 1986.
103. W. F. Gabriel, "Adaptive processing array systems," *Proc. of the IEEE*, vol. 80, no. 1, pp. 152–161, January 1992.
104. S. P. Applebaum, "Adaptive arrays," *IEEE Trans. Antennas and Propagation*, vol. AP-24, no. 5, pp. 585–598, September 1976.
105 R. J. Mailloux, *Phased Array Antenna Handbook*, Norwood, MA: Artech House, 2005.
106. M. Zatman, "Digitization requirements for digital radar arrays," in *Proceedings of the 2001 IEEE Radar Conference*, May 1–3, 2001, pp. 163–168.
107. G. H. C. van Werkhoven and A. K. Golshayan, "Calibration aspects of the APAR antenna unit," in *IEEE International Conference on Phased Array Systems and Technology*, May 21–25, 2000, pp. 425–428.
108. J. K. Mulcahey and M. G. Sarcione, "Calibration and diagnostics of the THAAD solid state phased array in a planar nearfield facility," *IEEE International Symposium on Phased Array Systems and Technology*, 1996, pp. 322–326, October 15–18, 1996.
109. M. Scott, "Sampson MFR active phased array antenna," in *IEEE International Symposium on Phased Array Systems and Technology*, October 14–17, 2003, pp. 119–123.
110. D. Slater, *Near-field Antenna Measurements*, Norwood, MA: Artech House, 1991.
111. H. M. Aumann, A. J. Fenn, and F. G. Willwerth, "Phased array antenna calibration and pattern prediction using mutual coupling measurements," *IEEE Trans. Antennas and Prop.*, vol. 37, no.7, pp. 844–850, July 1989.
112. E. Brookner, "Phased arrays and radars – past, present, and future," *Microwave J.*, vol. 49, pp. 24–46, January 2006.
113. R. M. Scudder and W. H. Sheppard, "AN/SPY-1 phased array antenna," *Microwave J.*, vol. 17, pp. 51–55, May 1974.
114. R. L. Britton, T. W. Kimbrell, C. E. Caldwell, and G. C. Rose, "AN/SPY-1 planned improvements," in *Conf. Rec. Eascon '82*, September 1982, pp. 379–386.
115. B. Walsh, "An eagle in the sky," *Countermeasures—The Military Electron. Mag.*, pp. 30–63, July 1976.
116. D. R. Carey and W. Evans, "The PATRIOT radar in tactical air defense," *Microwave J.*, vol. 31, pp. 325–332, May 1988.